

Chapter 3

Soil Water Budget and Drought Stress



Heike Puhlmann, Paul Schmidt-Walter, Peter Hartmann,
Henning Meesenburg, and Klaus von Wilpert

3.1 Introduction

The water budget of forest ecosystems is fed by precipitation. Loss into the atmosphere results from direct evaporation from the soil, transpiration, which is far more significant in forests due to their large crown-surface area, and evaporation from interception. The climatic processes governing these types of evaporation are air vapour pressure deficit, air temperature and convective water vapour transport. Another factor influencing the water budget occurs through soil water seepage, which is controlled mainly by the texture of the soil, its rock content and its bulk density. A certain amount of water is stored in the soil depending on texture, bulk density, carbon content, rock content and thickness of the soil layer. In most soils, except for very clayey and very sandy soils, the predominant part of the stored water is available to plants (available water capacity). The third factor determining the distribution and flow of water in the soil is vegetation. On the one hand, a considerable part of rain water is retained by the tree canopy and may evaporate directly from there (interception). On the other hand, water uptake by roots and transpiration influence the soil water budget of forest sites. This shows that, in addition to climatic processes, water-holding capacity and water conductivity of the soil as well as interactions between soil properties and vegetation properties (e.g. regarding root distribution) substantially determine and vary the water budget.

The water phase of the soil is the space in which the solution, exchange and transport processes take place that dictate most soil functions. Furthermore, water availability is a central property for the growth and productivity of forests. The

H. Puhlmann (✉) · P. Hartmann · K. von Wilpert
Forest Research Institute Baden-Württemberg, Freiburg, Germany
e-mail: heike.puhlmann@forst.bwl.de; peter.hartmann@forst.bwl.de

P. Schmidt-Walter · H. Meesenburg
Northwest German Forest Research Institute, Göttingen, Germany
e-mail: paul.schmidt-walter@nw-fva.de; henning.meesenburg@nw-fva.de

reaction equation of photosynthesis shows that water and carbon dioxide are the central components of plant growth. Seepage water flux is the transportation route for substances between the atmosphere, the soil and the hydrosphere. These are substances added by the rain such as nitrogen compounds, as well as reaction products of soil acidification such as aluminium and manganese ions. This shows that the seepage water flux substantially determines how well a soil acts as a filter. Because nearly all plant nutrients are taken up from the soil solution, there is a close connection between forest nutrition and the water budget. For example, a latent potassium deficiency becomes acute on clayey sites during and after a dry period. The reason for this is the accumulation of nutrients inside soil aggregates where they are difficult to access for plant roots (von Wilpert and Hildebrand 1997). Thus, the water budget plays an important role in the soil's ability to provide nutrients for the forest.

To avoid overlapping with other chapters of this book, the water budget of forests will be treated in this chapter by focusing on the direct effects of water availability. To achieve this, soil properties and soil processes are prioritized over climate and vegetation properties, all of which determine the water budget. The aim is to identify in what way water flow and availability are affected by the variability of soil properties. This analysis was done largely on the basis of soil data in the NFSI data set. Soil hydraulic properties such as water retention and water conductivity were derived from measured and estimated soil properties using pedotransfer functions (PTFs) (Puhlmann and von Wilpert 2011, 2012); see Sect. 3.2.1. Additionally, the depth profiles of fine roots for each of the NFSI profiles were estimated in a correlation analysis between fine root density (FRD) and soil properties (Hartmann and von Wilpert 2014); see Sect. 3.3.

Capacitive and dynamic water budget parameters for all NFSI profiles are derived from water budget modelling using LWF-Brook90. For the predominant part of the analysis, the forest stand properties (age, tree species composition, degree of canopy cover) were kept constant in order to clearly identify the significance of the individual soil properties for the result of the water budget modelling at the soil profiles. The vegetation properties described in the NFSI database are exemplarily included in the model for the purpose of comparison only in a last step of the analysis.

Static and dynamic drought stress characteristics were derived from water budget modelling in the concluding paragraph. They are discussed in reference to their ecological relevance on the basis of empirical data on tree growth (inter- and intra-annual tree-ring characteristics) and on mortality in Chap. 3. With this, the NFSI data are made available for comprehensive analyses in climate impact research. The model results are, of course, also applicable in a number of other applications such as predictions about seepage water output. In several federal states (Baden-Wuerttemberg, Bavaria, North Rhine-Westphalia, Rhineland-Palatinate and Saxony), concrete model developments are currently in progress to advance and objectify traditional, analogue site mapping. Because the identification of the water budget in all previous site mapping operations occurred in relative ordinal scales, it is neither possible to derive quantitative information on the water budget from the site maps nor to dynamically fit the site maps to changing climatic conditions (Gauer and Kroiher

2012). Therefore, quantitative and dynamic modelling of the water budget plays a central role when developing model-based site mapping procedures. The NFSI data is, in principle, suitable for that purpose—especially the measured physical soil parameters. The measuring network of the NFSI with its 2430 points does not represent Germany's forested area with its 11.1 million ha for detailed analyses properly; the mean density of the grid is approximately 6.8×6.8 km. If, however, multivariate estimation models with sufficient explanatory power are created on the basis of regression relations between measured soil parameters and terrain predictors, it is possible to create water budget models using estimated soil information (Zirlewagen and von Wilpert 2011) and link them to polygons of the forest site survey. The regression models will deliver more realistic results when incorporating the data set of all the German states, because the spatial density of measured soil parameters as well as corresponding co-variables (e.g. terrain attributes) becomes higher than would be possible on the level of single states. In this way, it is possible to substitute the ordinal, qualitative assessment of the site water budget of the individual forest site survey systems in the different federal states with modelled, time-variant quantitative information about the site water budget. Apart from methodological homogenization between the federal states, this would make the states' forest site survey systems also sensitive to climate.

3.2 Soil Properties as Input for Water Budget Modelling

Soil properties are input parameters for estimating and modelling the water budget of soils. They are included in the parameters of the NFSI II or can be derived from the information given in the NFSI. Especially with regard to physical soil characterization, the scope of the obligatory NFSI II parameters was extended significantly compared to the preceding inventory, and the measuring of parameters such as bulk density (using sampling rings or volume replacement samples), skeletal fraction (by volume replacement), texture (% S, U, T using the Köhn-Pipette or Lasersizer method) and carbon content (by element analysis) was required. For parameters, where measuring is extensive work such as counting fine root density with spatially high-resolving counting frames, most states still used estimated data; more precise counts were only done in Baden-Wuerttemberg. In addition to depth-related measured data, horizon-related estimated data regarding, e.g. texture, rock content and bulk density was collected in each case. Water retention and water conductivity, the two soil hydraulic properties required as input to soil water models, can be derived from these baseline pedological data only by using PTFs.

This chapter gives a description of regional variations in the mentioned measured and estimated physical soil parameters and of measurement and/or estimated accuracy.

The best available quality of the soil input data should be applied for modelling the water budget, i.e. the measured data (measured texture data, bulk density, etc.). However, because this data is not available in all states and only for certain depths,

the estimated data from the profile descriptions must be included to have a homogeneous database. It would be theoretically possible and necessary to consolidate the information from both data sources (estimated and measured) and to harmonize it with regard to survey artefacts (e.g. systematic bias between different estimating methods). Related harmonization work in individual states (e.g. Baden-Wuerttemberg) showed that this is a labour-intensive process and due to high heterogeneity among the states not possible to conduct nationwide within the framework of NFSI II. Therefore, for the federal soil report, measured data were used from depths in which they were available, and horizon-related estimated data were used where they were not.

3.2.1 Estimating Soil Hydraulic Functions Using Pedotransfer Functions

3.2.1.1 Introduction

Measured data on soil hydrological properties such as available water capacity (AWC) and the parameters for retention and conductivity functions at the NFSI plots were not all collected due to the high cost of measurement. For the characterization of the water budget, they have to be deduced indirectly using PTFs from the measured soil physical properties (texture, bulk density, carbon and humus content). The AWC shows the soil's ability to store water available for plants. Generally, this is specified by the difference between the volumetric water content at a soil water potential of -60 hPa (field capacity, pF 1.8) and $-16,000$ hPa (permanent wilting point, pF 4.2) and can be used for the static characterization of the water budget of a forest site. The parameters for the retention (van Genuchten 1980) and conductivity (Mualem 1976) models—abbreviated as MvG parameters below—are input parameters for process-based water budget models such as LWF-Brook90 (Hammel and Kennel 2001), which was used in this report (see Sect. 3.3).

A number of different PTFs for estimating characteristic soil hydraulic functions can be found in the literature. There have already been various projects and publications on the validation of PTFs for soil hydraulic characteristics in the past; especially the thorough works by Hangen and Scherzer (2004), Schramm et al. (2006), Mellert et al. (2009) and Russ and Riek (2011) should be mentioned in this context. However, the mentioned studies could not yet include newer developments such as the one by Puhlmann et al. (2009) and Puhlmann and von Wilpert (2011). In addition to that, many authors point out that the quality of the prediction is only valid for certain regions due to the geographical origin of the measured data used for validation or that some soil textures are underrepresented due to an insufficient number of samples. The results therefore do not allow any conclusions about the choice and application of the examined PTFs for the soils at the NFSI plots. In order to assist in choosing a PTF from the currently available PTFs, an individual study on

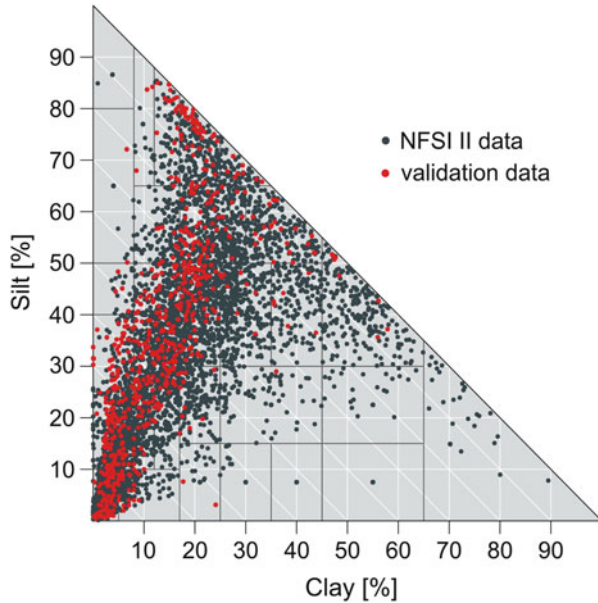
the basis of an extensive data set was conducted. That data was collected on forest sites in the whole of Europe and covers a wide range of soil types.

3.2.1.2 Materials and Methods

The data set available for PTF validation comprises a total of 2075 retention curves of mineral soil horizons, 130 retention curves of organic horizons as well as 866 samples where the saturated conductivity was measured. In addition to the target variables (retention curves, saturated hydraulic conductivity), the corresponding physical/chemical soil parameters (grain size fractions, bulk density and carbon/humus content) were available. These data are necessary for estimating AWC and MvG parameters using PTFs and for comparing them with the measured values. The data were obtained from the European Level II monitoring network (ICP Forests) and the forest research institutions and universities in Göttingen, Freiburg, Freising, Eberswalde and Graupa. It was ensured that no data sets were used that have already been incorporated in the development of the examined PTFs. In many cases, the sample rings for the retention curves did not come from the same soil profile as the physical/chemical soil parameters, only from the same test site. Because of these uncertainties, the decision was made to also exclude those measurements from the analyses and to only use samples where the input data for the PTF and the target variables originate from the same soil profile and horizon. By applying these restrictions, the data basis for validating the PTFs for the retention curve was reduced to 1641 mineral soil samples. One thousand four hundred twelve samples remained for the validation of the AWC, because not all retention curves contained information on the permanent wilting point and the AWC could therefore not be calculated. Figure 3.1 shows the distribution of the remaining retention curves inside the soil texture triangle; the samples of the NFSI II data set are shown for comparison.

Table 3.1 lists the examined PTFs and their abbreviations used below, as well as remarks and adjustments made during their application in this study. Which examined PTFs were chosen is based on the work of Hangen and Scherzer (2004) who, by means of extensive literature research, identified PTFs that seemed especially suitable for deriving hydraulic properties of forest soils. Two types of PTFs can be distinguished. One type of PTF predicts the water content for certain soil water potentials, typically for pF 1.8 (field capacity) and pF 4.2 (permanent wilting point). Because these PTFs predict fixed points on the retention curve, they are also called point PTFs. The tabular approaches by Wessolek et al. (2009) and Teepe et al. (2003) examined in this analysis fall into this category. Parametric PTFs, on the other hand, predict the parameters of retention models such as the van Genuchten model. With a water retention model, the water content can be predicted continuously as a function of the soil water potential. The regression functions by Wösten et al. (1999), Puhmann and von Wilpert (2011), Vereecken et al. (1989) and Teepe et al. (2003) are of this type. Tabular PTFs that list mean MvG parameters for different texture and density combinations also fall into this category, e.g. the PTF

Fig. 3.1 Distribution of retention data in the texture triangle



Teepe.TexTRD or the approach according to DIN 4220 (2008–2011) which was modified for this examination.

In addition to these modifications, adjustments were made to the PTF of Wessolek et al. (2009), as well as to the PTFs *Teepe.TexTRD* and *Teepe.KGA*. It turned out that for the latter, the values for the parameter α with the specified unit (kPa^{-1}) of the MvG curves do not fit to the table values for volumetric water content at field capacity (FC) and permanent wilting point (PWP). It did, however, produce results consistent with the table values when changing the unit for α to hPa^{-1} . Therefore, the α -values were multiplied by 10. The values of the lowest bulk density (TRD) class ($\text{TRD} < 1.2 \text{ g cm}^{-3}$) were not considered in the PTF *Wessolek.TexTRD*, because very high humus contents can often be found in horizons of forest soils in this TRD class. Accounting for humus content led in this TRD class to a significant overestimation of the total pore volume, the FC and the AWC. It turned out that, for soil samples from the TRD class 1.1, the increased water storage is already sufficiently reflected by the large humus content. Accordingly, samples with a TRD lower than 1.2 g cm^{-3} were assigned to the TRD class 1.3 when applying the PTF of *Wessolek.TexTRD*.

To objectively assess the quality of prediction of the individual PTFs, statistical goodness-of-fit measures were calculated based on the difference between estimated

Table 3.1 Overview of the examined pedotransfer functions for available water capacity (AWC)

Description/ literature source	Type/ calculation	Input parameters	Comments/adjustments
Wessolek. TexTRD (Wessolek et al. 2009)	Point PTF, Ks/table	Texture class (KA5), TRD class, humus class	Tables 3 + 5. Density class 1.1 was not considered, and samples with TRD < 1.2 g cm ⁻³ were assigned level 1.3. For undefined combinations of TRD and texture class, the value of the bordering density level of the respective texture class was assumed
DIN4220. TexTRD (DIN 4220 2008–2011)	Param. PTF/ table	Texture class (KA5), TRD class	MvG parameters from Table 10 in Wessolek et al. (2009) were adjusted according to the water potential/water content values from Table A1 of the DIN 4220, so that MvG parameters were available separately for individual texture and TRD classes
Teepe.KGA (Teepe et al. 2003)	Point PTF + param. PTF/equation	%S/%U/%T, TRD	MvG- α was multiplied by 10
Teepe.TextRD (Teepe et al. 2003)	Point PTF + param. PTF/table	Texture class (KA5), TRD class, Corg	MvG- α was multiplied by 10; supplementing of the missing values for air capacity, AWC and PWP for sands from DIN 4220. Minimum %S, %U, %T limited to 0.5%
PUH2.KGA (Puhmann and von Wilpert 2011)	Point PTF + param. PTF, Ks/equation	%S/%U/%T, TRD, Corg	
Vereecken.KGA (Vereecken et al. 1989)	param. PTF/ equation	%S/%U/%T, TRD, Corg	Adjustment of %S and %U to the grain size boundary at 50 μ m through log-linear interpolation of the grain size curve
Hypres.KGA (Wösten et al. 1999)	Param. PTF, Ks/equation	%S/%U/%T, TRD, humus con- tent, top-/subsoil	Minimum TRD limited to 0.5 g cm ⁻³ , minimum %U, %T to 0.5%. All samples taken from a depth below 30 cm were classified as subsoil. Adjustment of the boundary between %S and %U as for Vereecken.KGA

and measured volumetric water content. Accuracy measures of predictions are the mean error (ME) and the mean absolute error (MAE):

$$ME = \frac{1}{n} \sum_{i=1}^n (\hat{y}_i - y_i) \quad (3.1)$$

$$\text{MAE} = \frac{1}{n} \sum_{i=1}^n (|\hat{y}_i - y_i|) \quad (3.2)$$

The ME as the arithmetic mean of all residuals (difference between estimate \hat{y} and measurement e) indicates systematic over- (positive values) and underestimations (negative values). In the ideal case of an unbiased prediction, ME takes a value of 0.

The precision of predictions was evaluated using the root mean squared error (RMSE):

$$\text{RMSE} = \sqrt{\frac{1}{n} \sum_{i=1}^n (\hat{y}_i - y_i)^2} \quad (3.3)$$

The RMSE quantifies the standard deviation of the residuals and therefore the absolute value of the total error that can be expected on average and ideally also takes a value of 0.

Pearson's correlation coefficient is a statistical measure for comparing individual measured retention curves with estimated ones using parametric PTFs. It is calculated as follows:

$$r = \frac{\sum_{i=1}^n (\hat{y}_i - \bar{\hat{y}})(y_i - \bar{y})}{\sqrt{\sum_{i=1}^n (\hat{y}_i - \bar{\hat{y}})^2 + \sum_{i=1}^n (y_i - \bar{y})^2}} \quad (3.4)$$

Thereby, \bar{y} and $\bar{\hat{y}}$ specify the mean values of measurement and estimate. In the case of perfect positive correlation, the different water contents of the individual points of soil water potential lie on a line with a positive slope, and r assumes a value of 1. The correlation coefficient can therefore be seen as a similarity measure of the progression and shape of two retention curves. Another similarity measure is Wilmot's index (w):

$$w = 1 - \frac{\sum_{i=1}^n (y_i - \hat{y}_i)^2}{\sqrt{\sum_{i=1}^n (|\hat{y}_i - \bar{y}|)^2 + (|y_i - \bar{y}|)^2}} \quad (3.5)$$

Multiplied with the correlation coefficient, Wilmot's w produces the confidence index (CI = $w * r$) that also takes a value of 1 when measurement and estimate are in perfect accordance. Values of >0.85 are seen as excellent predictions, values of >0.75 as good and values of ≤ 0.75 as less than good (de Camargo and Sentelhas 1997).

The ME and the RMSE are used in the assessment of the prediction quality for water contents of individual water potential levels (1, 10, 60, 100, 330, 1000, 2500, 5000, 16,000 hPa) and available water capacity. For evaluating parametric PTFs for the retention curve, the CI, the RMSE and the ME are calculated for the whole range of soil water potential. In order to make conclusions about the approximate distribution of the quality criteria of the PTF over a range of soil textures, the quality criteria are calculated separately for the 11 soil texture groups of the German soil texture classification system (Ad-Hoc AG–Boden 2005). After that, the PTFs are ranked for each quality criterion. For the available water capacity, the differences between PTF estimates and measured values are added to the texture triangle as isolines. In this way it is possible to make conclusions about the PTFs' performance for different texture groups. The goal is to identify which PTF is best suited for the NFSI II soil data. To achieve this, the mean rank for each quality criterion is calculated from the ranks of the quality criteria of the individual soil texture groups. This mean rank is weighted using the respective number of observations in the NFSI II data set. Finally, simple not-weighted mean values are produced from these, establishing a final rank order for the PTFs.

3.2.1.3 Results and Discussion

Figure 3.2 shows the deviation between estimated and measured water contents for each PTF as a function of the soil water potential, separated according to soil texture groups. Additionally, the ME is plotted for the various water potential classes, which makes it possible to recognize systematic errors. The graphical display of the results for clayey loams (tl), loamy clays (lt) and sandy silts (su) was refrained from because of the small number of observations. The quality criteria MAE, RMSE and CI which integrate over all pF levels can be found in Table 3.2 for all soil texture groups. The systematic errors of individual soil texture groups are listed in Table 3.2 and were calculated as mean values of the MAE in order to not cancel out opposing deviations between the individual water potential classes.

In general, the variation and therefore the RMSE decrease with increasing water potential due to decreasing water contents. This becomes clear when looking at the narrowing box and whisker ranges (Fig. 3.2). It seems that the characteristic progressions of the retention curves of the individual soil texture groups cannot be reconstructed satisfactorily by each of the investigated PTFs. For example, the PTFs *Hypres.KGA* and *Vereecken.KGA* tend for nearly all soil texture groups to estimate a sharper decrease in water content than the measured data suggest. This becomes apparent from overestimated water contents at low water potentials in combination with underestimated water contents at high water potentials (Fig. 3.2) and can also be seen in the low goodness-of-fit measures (Table 3.2).

The curvature of the van Genuchten retention model depends on the parameters α and n . Since the water content close to saturation and the water content at the permanent wilting point are predicted relatively well, it seems reasonable to hold insufficient estimates of the α and n parameters responsible for the weaknesses of the

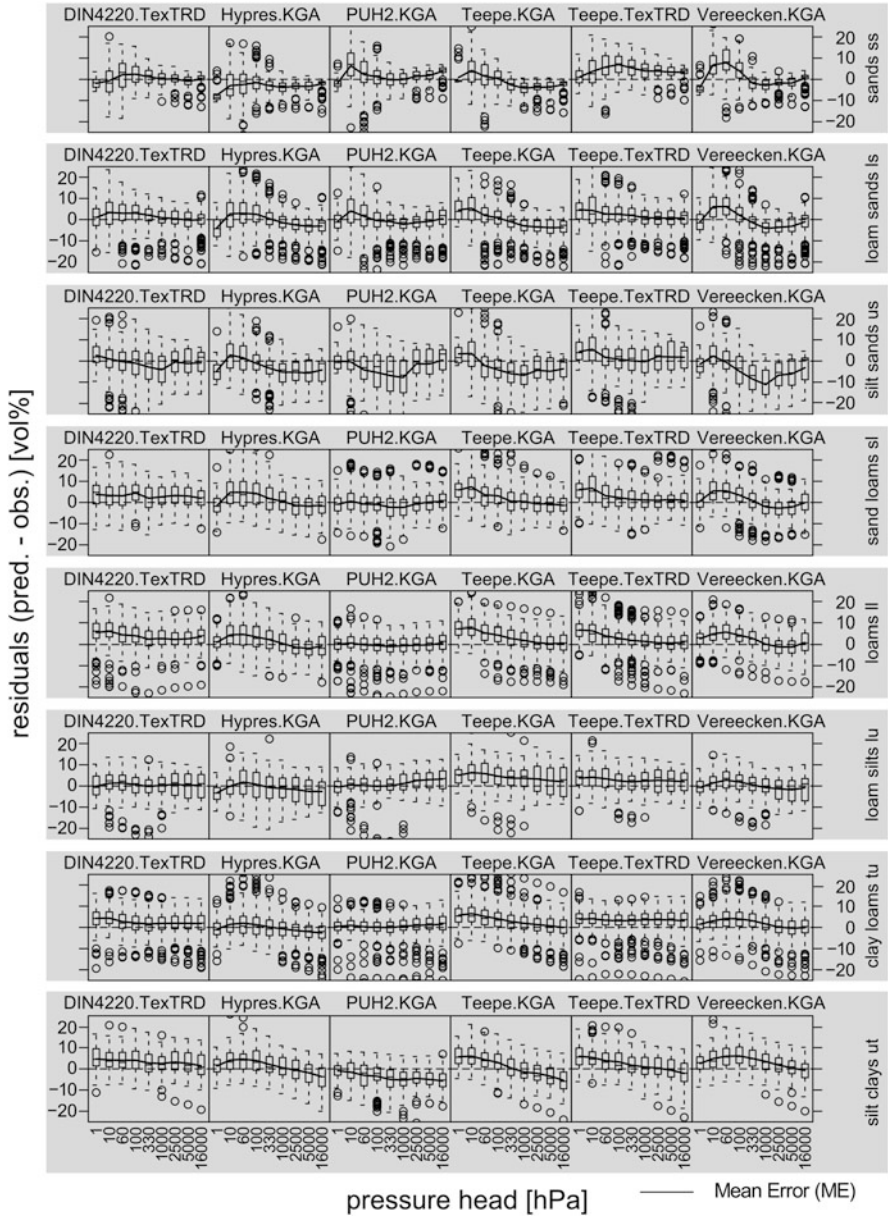


Fig. 3.2 Deviations (boxplots) and mean deviation (solid lines) between PTF estimates and measured water contents (in vol%) as a function of matric potential, divided into soil texture groups

two PTFs. Except for silty-clayey substrates (texture groups lu, tu), the PTFs do not produce satisfactory predictions for the retention curves of the validation data set.

Table 3.2 Mean absolute error (MAE, vol%), root mean squared error (RMSE, vol%) and confidence index (CI, dimensionless) over all pF levels for all soil texture groups

Soil texture class	Sands			Loams			Silt			Clays			Mean
	ss	ls	us	sl	ll	tl	su	lu	tu	ut	lt		
Soil texture group	132	400	136	272	261	1	4	79	260	82	14		
<i>N</i>													
RMSE (vol%)													
<i>DIN4220.TexTRD</i>	5.0	5.9	7.9	6.5	6.7	8.8	8.0	6.2	5.7	6.9	5.3	6.6	
<i>Hypres.KGA</i>	5.6	6.4	7.6	7.3	6.4	3.6	6.1	7.1	5.8	6.5	5.9	6.2	
<i>PUH2.KGA</i>	5.9	6.0	10.1	5.8	4.9	5.4	6.0	5.6	4.6	7.0	13.4	6.8	
<i>Teepe.KGA</i>	5.6	6.1	8.8	7.3	7.0	5.5	7.2	8.0	6.7	6.9	8.2	7.0	
<i>Teepe.TexTRD</i>	7.0	6.3	7.9	7.5	6.7	5.9	7.8	6.3	5.8	6.8	8.8	7.0	
<i>Vereecken.KGA</i>	6.5	6.6	9.9	6.6	5.9	4.5	5.3	5.7	5.7	7.1	5.8	6.3	
MAE (vol%)													
<i>DIN4220.TexTRD</i>	1.1	1.6	1.6	3.1	3.9	8.5	4.8	0.6	2.5	3.3	2.9	3.1	
<i>Hypres.KGA</i>	3.3	2.5	3.8	2.4	2.3	3.1	3.0	1.6	1.4	2.5	3.9	2.7	
<i>PUH2.KGA</i>	2.1	1.4	3.1	1.0	0.5	4.2	3.9	1.2	0.6	3.8	12.8	3.1	
<i>Teepe.KGA</i>	2.6	3.1	4.3	2.6	3.5	5.2	6.0	4.1	3.1	3.5	7.0	4.1	
<i>Teepe.TexTRD</i>	4.2	2.1	2.1	2.7	2.9	5.1	5.9	2.8	3.5	2.7	6.6	3.7	
<i>Vereecken.KGA</i>	3.5	3.2	5.0	2.6	2.7	3.9	3.2	1.3	2.0	3.4	2.4	3.0	
CI (-)													
<i>DIN4220.TexTRD</i>	0.82	0.85	0.74	0.81	0.78	0.81	0.82	0.81	0.80	0.60	0.49	0.76	
<i>Hypres.KGA</i>	0.81	0.83	0.81	0.78	0.78	0.95	0.87	0.77	0.78	0.66	0.56	0.78	
<i>PUH2.KGA</i>	0.78	0.83	0.63	0.82	0.83	0.87	0.91	0.85	0.84	0.61	0.33	0.76	
<i>Teepe.KGA</i>	0.83	0.87	0.76	0.81	0.80	0.91	0.92	0.78	0.79	0.65	0.49	0.78	
<i>Teepe.TexTRD</i>	0.76	0.84	0.76	0.79	0.80	0.89	0.87	0.84	0.81	0.65	0.31	0.76	
<i>Vereecken.KGA</i>	0.77	0.83	0.70	0.82	0.82	0.93	0.91	0.85	0.81	0.64	0.53	0.78	

The best values for individual quality criteria in the respective soil texture group are highlighted in bold. Below the soil texture group symbols, the number of samples within each group is given

The PTFs *Teepe.TextRD* and *Teepe.KGA* produce slightly better results. These seem to have their strengths in clayey-silty textures, for which, judging by the CI, the shape of the retention curve can be predicted relatively well. However, the water contents are overestimated for nearly all texture groups, especially in the range of low soil water potentials, and come with a wide uncertainty range. For these reasons and on the basis of the mean RMSE and MAE values, they have to be rated as the least suitable PTFs for predicting the retention properties of forest soils.

Using objective criteria, the best PTF found for predicting the retention function of the examined soil samples, is the PTF *PUH2.KGA* (Table 3.2). It provides nearly unbiased, high-precision estimates for the retention function (Fig. 3.2) over a wide range of textures. With *PUH2.KGA*, only the prediction of retention properties of sands seems problematic. The water contents of the silt sands (us) are significantly underestimated for medium water potentials and come with great uncertainties. Contrary to the loamy-silty substrates, the water contents of the pure sands (ss) and loam sands (ls) at low water potentials as well as the water content at the permanent wilting point ($-16,000$ hPa) are in part largely overestimated. Additionally, there is a significant underestimate of water retention in clayey soils (ut, lt).

A PTF that, in contrast to all other PTFs, provides satisfactory estimates of the retention function over all soil texture groups, is the PTF *DIN4220.TextRD*. It is, for example, the only PTF that estimates the retention of pure sands accurately and also provides robust, although slightly too high, estimates for clayey soils. In the loamy-silty range (sl, ll, lu, tu), *DIN4220.TextRD* is less precise compared to other PTFs and tends to have slightly high, but satisfactory, estimates with a mean RMSE of 6.6 vol% and a MAE of 3.1 vol%. The mean CI over all soil texture groups with a value of 0.76 is also slightly lower than that of other PTFs. This can be explained by a generally larger variation of the deviations of tabular PTFs. On average, however, the shape of the retention curve can be satisfactorily represented. This becomes also clear when looking at the generally uniform distribution of residuals over the entire range of water potentials.

The estimates for the AWC show a picture similar to the estimates for the retention curve. *Hypres.KGA* and *Vereecken.KGA* overestimate the AWC in all soil texture groups on average by approx. 6 vol% (Table 3.3). This was to be expected considering the systematic overestimates of the water content at low, and the underestimates at high water potentials described in the previous paragraphs. Both PTFs show on average the highest uncertainties (*Hypres.KGA*, 9.9 vol%; *Vereecken.KGA*, 8.4 vol%) and will be rated as least suitable for estimating the AWC of forest soils. Slightly better results are found for the PTFs *Teepe.KGA* and *Teepe.TextRD*. Their estimates also show large uncertainties, but with a mean ME of 3.6 vol% (*Teepe.TextRD*) and 4.5 vol% (*Teepe.KGA*), they provide less biased estimates. The PTFs *DIN4220.TextRD* and *Wessolek.TextRD* show similar results due to originating from the same source, whereby the point PTF *Wessolek.TextRD* includes the humus contents of the samples, while *DIN4220.TextRD* does not. This is possibly the reason for the RMSE of the PTF.

Wessolek.TextRD with 6.5 vol% being slightly lower than the one of *DIN4220.TextRD* (RMSE 7.2 vol%). Both PTFs slightly overestimate the AWC by 3.4 vol%.

Table 3.3 Mean error (ME, vol%) and root mean squared error (RMSE, vol%) of the estimate of the available water capacity for all soil texture groups

Main soil texture	Sands			Loams			Silt			Clays		Mean
Soil texture group	ss	ls	us	sl	ll	tl	su	lu	tu	ut	lt	
	61	250	67	185	193	0	4	49	210	44	6	
RMSE (vol%)												
<i>DIN4220. TexTRD</i>	7.2	7.2	8.6	7.0	5.0		6.1	7.6	5.6	7.3	10.7	7.2
<i>Hypres. KGA</i>	8.7	10	9.8	9.5	8.0		9.2	10.2	7.8	11.0	14.8	9.9
<i>PUH2. KGA</i>	11.5	7.5	6.9	6.1	4.2		3.2	7.5	5.2	5.5	7.6	6.5
<i>Wessolek. TexTRD</i>	6.3	7.1	8.3	6.4	4.5		6.1	7.7	5.5	7.9	12.4	7.2
<i>Teepe. KGA</i>	7.9	8	7.6	7.0	5.5		5.9	7.8	6.1	9.9	14.3	8.0
<i>Teepe. TexTRD</i>	7.6	7.2	6.5	7.3	6.7		3.5	7.9	5.7	10.6	13.1	7.6
<i>Vereecken. KGA</i>	9.7	8.9	8.6	7.9	6.6		9.0	7.8	6.9	9.4	9.4	8.4
ME (vol%)												
<i>DIN4220. TexTRD</i>	3	2.6	4.2	1.4	0.6		5.2	0.7	0.9	5	10.4	3.4
<i>Hypres. KGA</i>	0.3	6.1	5.0	4.7	5.4		8.5	4.2	4.5	9.7	14.0	6.2
<i>PUH2. KGA</i>	-9.0	-3.6	-2.5	-1.0	0.0		2.7	-2.2	0.0	2.4	-3.2	-1.6
<i>Wessolek. TexTRD</i>	-1.0	2.4	5.2	2.6	1.3		5.2	0.1	0.6	5.7	12	3.4
<i>Teepe. KGA</i>	4.1	3.9	2.1	2.4	3.1		5.2	0.0	1.8	8.5	13.4	4.5
<i>Teepe. TexTRD</i>	3.6	2.9	1.2	2.5	2.9		2.2	-0.7	0.0	8.4	12.6	3.6
<i>Vereecken. KGA</i>	5.9	6.5	5.6	5.1	4.9		8.8	2.8	4.2	8.1	8.2	6.0

Highlighted in bold are the best values of the quality criteria in the respective soil texture group

In contrast to all other PTFs that on average overestimate the AWC of all soil texture groups by varying degrees, *PUH2.KGA* on average slightly underestimates AWC (-1.6 vol%). In the same way as for the retention curve, this PTF provides the most precise and least biased estimates for all soil texture groups.

Figure 3.3 shows the differences (smoothened using a generalized additive model) between the estimated AWC values using the PTFs *PUH2.KGA* (Fig. 3.3a) and *Wessolek.TexTRD* (Fig. 3.3b) and the measured AWC values in the texture triangle. Areas with the same systematic error are framed by isolines (Table 3.3),

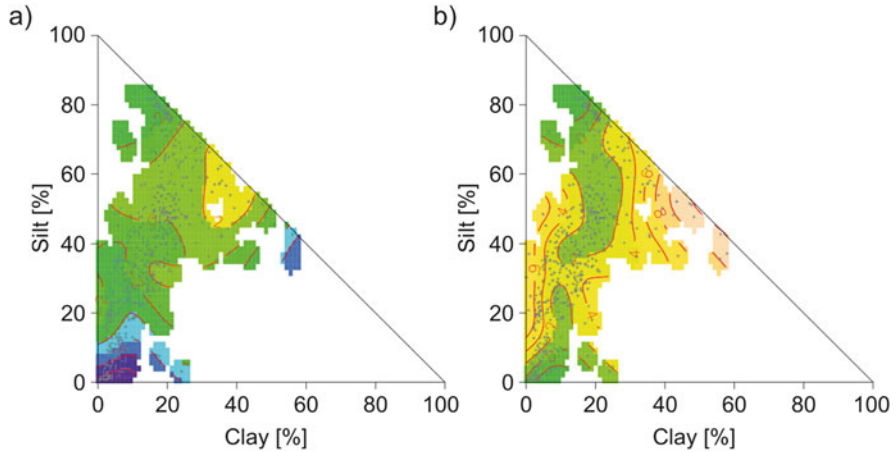


Fig. 3.3 Isoline diagrams generated using a generalized additive model of the smoothed deviations of estimated and measured available water capacity (vol%) as a function of the clay and silt content. Displayed are the pedotransfer functions PUH2.KGA (A) and Wessolek.TextRD (B). Green and yellow-green areas represent deviations in the range of ± 2 vol%, yellow to yellow-brown areas indicate systematic overestimates and blue-green and blue areas indicate an underestimate of the available water capacity

whereby blue areas indicate underestimations of ≤ 4 vol%, and yellowish-brown areas overestimations of > 4 vol%. As shown already in Table 3.3, systematic deviations of the PTF *PUH2.KGA* lie between -2 vol% and $+2$ vol% in large areas of the texture triangle, the smallest deviations appearing in silty-clayey areas. With decreasing silt and clay content, the PTF increasingly underestimates the AWC, at first only slightly, but then strongly when the sand content becomes larger than 60%. In this way, silt contents of $< 10\%$ and $< 5\%$ lead to systematic underestimates of the AWC of more than 8 vol% and more than 10 vol%, respectively. Because the validation data set contains many samples within this texture range, it can be assumed that this trend originates from a systematic error of the PTF *PUH2.KGA*, because the calibration data set used for developing the PTF contained only few pure sand and silty sand samples. The group of loamy clays was also underrepresented in the data set for the development of *PUH2.KGA*, and there are indications for a substantial underestimation of the AWC. However, within the validation data set, the number of samples with clay contents of $> 50\%$ is too low for making serious conclusions about this response.

Contrary to *PUH2.KGA*, Fig. 3.3b shows a systematic overestimate of 8–12 vol% of the PTF *Wessolek.TextRD* for the clayey silts and the clayey loams. The least biased estimates lie, for the largest part, within the texture ranges that also have the highest sample density in the NFSI data collection. They extend from the pure and loamy sands to the sandy loams to the silts. Several areas, despite of having a sufficient amount of samples, are affected by significant overestimates in the range of 4–6 vol%, such as the silty sands and the sandy silts as well as regular loams and

silty clays. This circumstance can be explained by higher uncertainties of *Wessolek.TexTRD* when compared to *PUH2.KGA* (Table 3.3). The biggest difference between PTFs *PUH2.KGA* and *Wessolek.TexTRD* exists within the pure sands and the silty sands, for which *Wessolek.TexTRD* estimates the AWC with deviations of <2%, while *PUH2.KGA* significantly underestimates the AWC in this range of textures.

3.2.1.4 Conclusions About Choosing the Appropriate Pedotransfer Function for the Water Budget Modelling

The final ranking of the PTFs is based on the quality criteria of Table 3.2 and shows that the most appropriate approach for estimating the retention curve for the depths used in the NFSI data set is the one by Puhlmann and von Wilpert (2011).

For the weighted overall ranking, low prediction quality of the numerous sandy substrates within the NFSI II data set is compensated for by very good prediction properties for loamy and silty substrates, which are very numerous within the data set as well. However, a PTF that is applied to such a diverse data set as the NFSI II is required to satisfactorily predict the retention function for all soil textures. Therefore, the PTF according to DIN 4220 (2008–2011) was finally chosen for the water budget model. This approach is only second choice by objective criteria (Table 3.4). It does, however, provide satisfactory results over a wide range of soil textures. In addition, for estimating the soil hydrological properties FC, AWC and PWP, the best approach according to objective criteria, the *Wessolek.TexTRD*, may be used without the values differing much from the values of the retention curve, because both PTFs are derived from the same source.

Table 3.4 Summary of overall ranking of the pedotransfer functions for the retention curve and the available water capacity, based on the ranking of the quality criteria of Tables 3.2 and 3.3

	Retention curve								AWC					
	Rank RMSE		Rank MAE		Rank CI		Mean rank		Rank RMSE		Rank ME		Mean rank	
<i>DIN4220.TexTRD</i>	2.4	(2)	3.1	(3)	3.7	(5)	3.1	(2)	2.6	(3)	2.6	(2)	2.6	(1)
<i>Hypres.KGA</i>	3.5	(3)	2.9	(2)	4.2	(6)	3.5	(3)	6.5	(7)	5.5	(6)	6.0	(7)
<i>PUH2.KGA</i>	2.4	(1)	2.0	(1)	3.0	(1)	2.5	(1)	2.5	(2)	3.0	(3)	2.8	(3)
<i>Wessolek.TexTRD</i>									2.0	(1)	2.6	(1)	2.3	(2)
<i>Teepe.KGA</i>	4.4	(5)	4.7	(6)	3.0	(2)	4.0	(5)	4.3	(5)	4.3	(5)	4.3	(5)
<i>Teepe.TexTRD</i>	4.5	(6)	4.4	(5)	3.6	(4)	4.2	(6)	4.2	(4)	3.4	(4)	3.8	(4)
<i>Vereecken.KGA</i>	3.7	(4)	3.9	(4)	3.4	(3)	3.7	(4)	5.2	(6)	5.8	(7)	5.5	(6)

The ranks of the quality criteria in the individual soil texture groups were weighted by the number of observations of the NFSI II within the respective soil texture group; the placement is shown in parentheses next to the ranks

3.3 Fine Root Distribution on NFSI Sites

Fine root distributions are essential for the parametrization of soil water budget models of forest sites, because they represent the link between the forest stand and the soil. However, the ideal for tree species-specific rooting patterns is not applicable in practice, because the actual fine root distribution patterns are strongly influenced by soil and site properties (Hartmann and von Wilpert 2014). Therefore, it is necessary to determine the actual depth distribution of fine roots or define reliable transfer functions for sites without any root information.

3.3.1 Fine Root Density Model

Using multivariable statistical analyses, correlation analyses were performed between the fine root density (FRD, measured in classes shown in the profile description according to Ad-Hoc AG–Boden (2005), converted into mean values of each class) as the target variable and soil and site properties as predictor variables. With the help of “boosted regression trees” (BRT), the principle parameters and their influence on FRD were identified. The final BRT model is a linear combination of all calculated regression trees. The quality of the model can be rated by correlation with the training and the validation data, as well as the remaining error. The influence of the individual parameters is interpreted using the percentage of the influence and the absolute effects on the model’s result. For the analyses, the “dismo” package of the statistical software “R” was used (Elith et al. 2008).

The final model was limited to the five most important parameters and has a good model quality (correlation training data, 0.701; correlation validation, 0.695). The effect of the individual parameters on the target variable FRD is displayed in Fig. 3.4. With a percentage of 62.2%, the parameter soil depth explains the largest part of the FRD, meaning that the maximum can be found in the topsoil, with a continuous decrease with soil depth. The humus content proved to be another important predictor. On the one hand, it is a result of root growth, especially in the subsoil, and on the other, it facilitates root penetration through loosening the soil structure. Alongside those parameters are also soil physical properties such as bulk density and available water capacity, as well as the relief parameter slope in direct relation with the FRD.

The approximate linear relationships within the model can be summed up in a PTF. To achieve this, a simple linear equation model was created. The resulting PTF for FRD in m dm^{-2} is (adjusted R -squared, 0.3973; $p < 0.001$; Fig. 3.4):

$$\text{FRD} = 11.63 - 0.084 \text{ soil}_{\text{depth}} + 3.22 \text{ humus}_{\text{class}} - 3.42 \text{ TRD} + 0.108 \text{ slope} + 0.095 \text{ AWC} \quad (3.6)$$

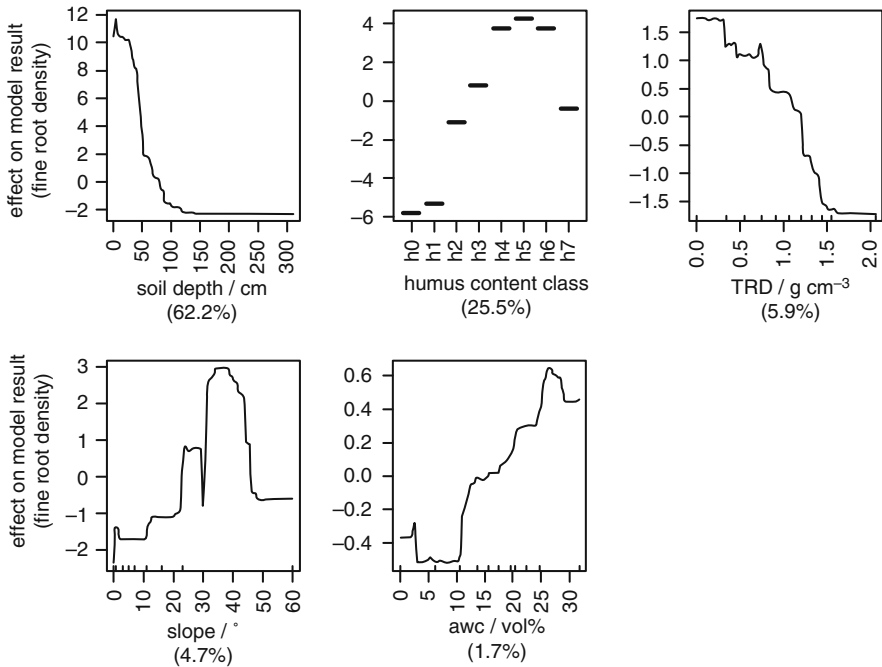


Fig. 3.4 Results of the “boosted regression trees” analysis: The fine root density in the horizon is the models’ target variable. The individual diagrams show the influence of the parameters (x -axis) on the modelled fine root density (y -axis). The percentage determines the weighting of the parameter in the model; soil_depth, depth of the horizons bottom edge (cm); humus = humus class according to Ad-Hoc AG–Boden (2005); TRD, bulk density, measured in different depths and converted to represent the specific soil horizon (g cm^{-3}); slope, slope on site ($^{\circ}$); AWC, available water capacity, measured in different depths and converted to represent the specific soil horizon (vol%)

In comparison with the BRT modelling, the PTF performs worse. But although being weaker, the PTF reaches a high model quality as well.

3.3.2 Continuous Fine Root Distribution

For parametrization of the root distribution in water budget models, continuous information on the FRD is required. To achieve this, the exponential function according to Gale and Grigal (1987) may be used. It calculates the depth-dependent, relative root distribution continuously using a shape parameter β (Fig. 3.5). This is especially reasonable for inhomogeneous data sets such as the NFSI II data set, because different data collection methods (Bavaria, estimation at soil auger samples; Baden-Wuerttemberg, counting fine roots in a 5 cm grid at the wall of the profile; rest

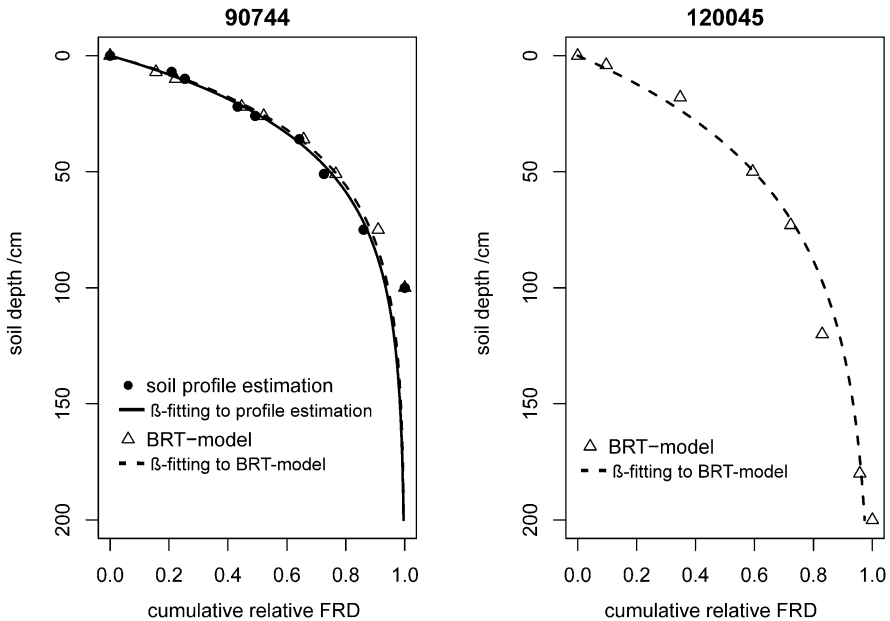


Fig. 3.5 Example of a good adjustment and congruency between estimated values, “boosted regression trees” model values and the respective adjustment to the β -model (left), and example of a site at which the β -model was adjusted to the “boosted regression tree” model values, because soil profile estimates were lacking (right)

of Germany, estimating at the soil profile) lead to different estimates of rooting intensities.

Figure 3.6a shows the number of fine roots (derived from the different estimating procedures) in the recorded root zone for all NFSI profiles. It can be noticed that above-average amounts of fine roots occur in Baden-Wuerttemberg, whereas in Bavaria the amounts are often extremely small. Despite the regional differences, the estimates of the FRD were used for further adjustment, since only the relative depth distribution was taken into account, and therefore, different classification procedures during profile description were “normalized”. Where there were no estimated values available, they were filled in with values from the estimates of the BRT. First, the FRDs per horizon were calculated ($\text{FRD} \times \text{thickness}$) and plotted as the cumulative sum on the lower end of the horizon and then fitted to the β -model according to Gale and Grigal (1987) with a non-linear optimization algorithm (Fig. 3.5):

$$Y = 1 - \beta^z \quad (3.7)$$

where Y is the cumulative relative FRD in depth z and β the parameter to be adjusted.

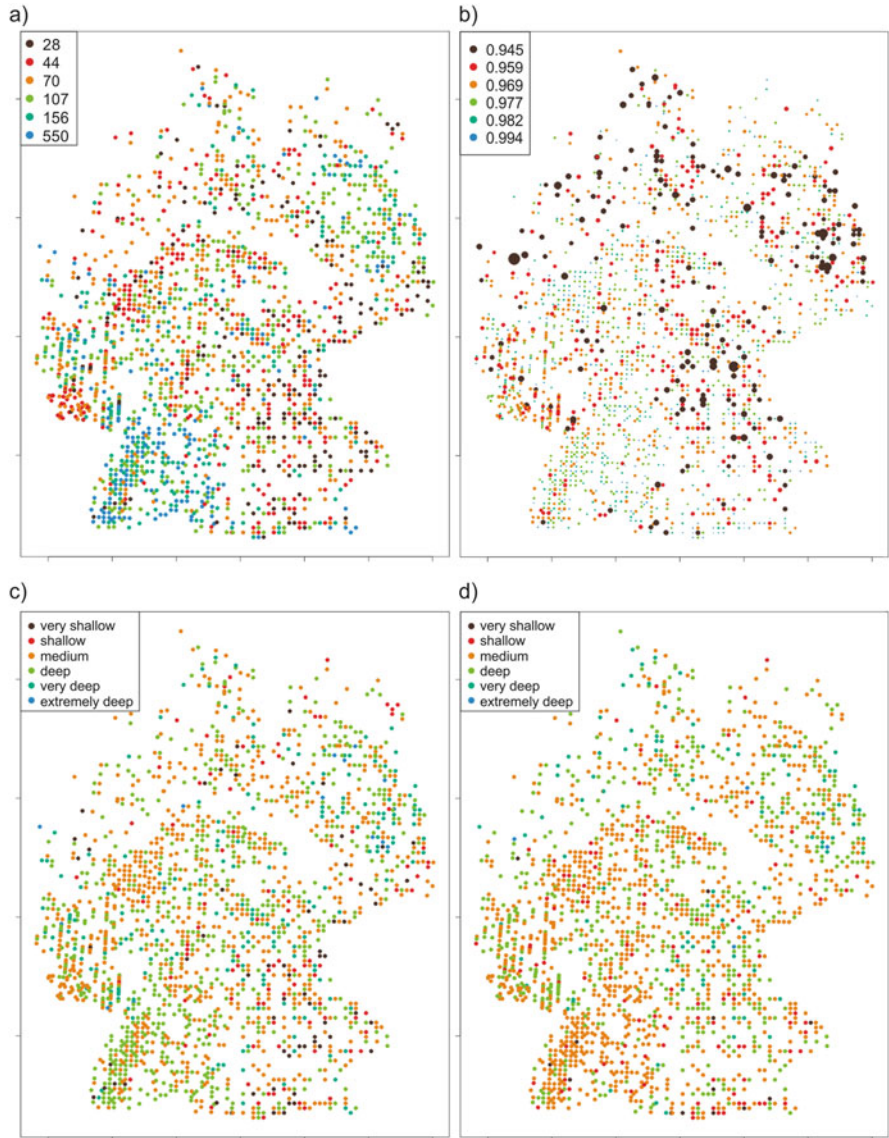


Fig. 3.6 Number of fine roots summed up over the whole soil profile to a width of 1 dm (a). The different colours define percentiles (10-25-50-75-90-100); β -values of the NFSI II profiles (percentiles 10-25-50-75-90-100). The size of the dots correlates with the β -value (b). Blue dots represent deep distributions, red shallow ones; RDefeff according to conventional definition (c); RDefeff, determined using the depth, in which 86% of the cumulative amount of fine roots are located according to the β -model (d)

The relative cumulative amount of fine roots can now be calculated for any depth using this function. The resulting β -values are shown in Fig. 3.6b, where high values represent deeper distributions.

3.3.3 *Effective Rooting Depth*

The effective rooting depth is a cautious estimation of the main rooting zone used in German forest soil classification, which can be derived from the lower limit of a FRD >2 fine roots per dm^2 according to AK Standortskartierung (2003). By this approach an overestimation of the effective rooting depth is avoided, because the least densely rooted zone in the subsoil is not taken into account. In our data, the effective rooting depth always coincides with the lower boundary of a horizon, because the FRD is defined for each horizon individually. This value is distorted to some extent, as a depth-dependent decrease in FRD can also be assumed within a horizon. Additionally, different data collection methods result in FRDs that are not comparable to each other (Fig. 3.6c). The estimates from the conventional approach reaffirm the differences between Baden-Wuerttemberg and Bavaria caused by different estimation methods.

In order to generate a uniform value for the β -model on the basis of the boundary Wf2/Wf1 (2 fine roots per dm^2) from the conventional model, the cumulative percentage Z was determined, for which the rooting depth from the conventional approach, $\text{RDeff}(\text{conv})$, can be reached best. This was done using a non-linear adjustment:

$$\text{RDeff}(\text{conv}) \sim \log(1 - Z)/\log(\beta) \quad (3.8)$$

This results in a value for Z of 86%, which will be used hereafter as the effective rooting depth according to the β -model, $\text{RDeff}(\beta \text{ 86\%})$ (Fig. 3.6d).

3.3.4 *Effect of Stand Type, Soil Class and Acidification*

The forest stand at the NFSI sites are in most cases no pure stands with one tree species only, rather stand types of different degrees of purity and mixed stands are defined. Hence, as the species origin of the fine roots was not determined, the following analyses always refer to the stand type and not a single tree species. The evaluation of the rooting space is based on the RDeff value (Fig. 3.6), which corresponds to the 86% depth in the β -model. No significant differences were found in the rooting depths for the individual stand types (Fig. 3.7). There is a wide variation in all stand types, with median values of approx. 60 cm. The stratification according to soil type also shows only small differences between the groups. Only the sandy soils poor in base cations show increased RDeff values,

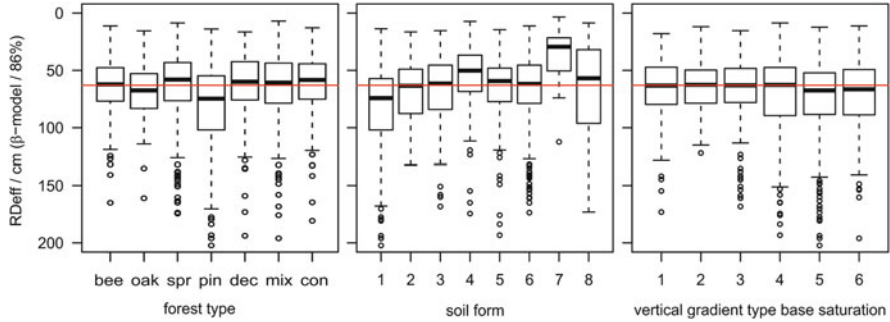


Fig. 3.7 Boxplots showing the effective rooting depth, R_{Deff} (β -model; see Eq. 3.8), stratified according to forest type, soil form (centre) and vertical gradient of base saturation (right); *bee* beech, *oak* oak, *spr* spruce, *pin* pine, *dec* deciduous forest, *mix* mixed forest, *con* coniferous forest; soil forms, 1 = sands poor in base cations, 2 = alluvial soils and gleys of wide river valleys, 3 = lowland soils and loess loams, 4 = limestone-derived soils, 5 = basic to intermediate soils originated from crystalline rock and pelosols, 6 = soils poor in base cations from crystalline rock, 7 = alpine soils, 8 = peat soils; vertical gradients, 1 = complete base saturation (100%) in the root space, 2–4 = base saturation decreasing with depth and qualitatively in the main root space with full base saturation in the subsoil, 5 = base depletion in the whole profile, 6 = increased base saturation in the humus/mineral topsoil by liming, classification according to Hartmann and von Wilpert (2016)

whereas in limestone-derived soils, and especially in alpine soils, several significantly reduced values appear. Surprisingly, the R_{Deff} values do not point towards an influence of an advancing acidification or of forest liming, as the stratification according to vertical gradients of base saturation shows.

3.4 Modelling Dynamic Water Availability in Forests

3.4.1 Model Description, Input Data, Parameterization and Target Variables

The water budget modelling for individual NFSI II points was carried out using the process-based forest hydrological simulation model LWF-Brook90 (Hammel and Kennel 2001), which is a further development of the model Brook90 (Federer et al. 2003). LWF-Brook90 calculates the water budget of a one-dimensional, multilayered soil profile with vegetation cover in daily resolution. Water transport in the soil is described by the Richards equation. Source and sink terms thereby include processes such as flow through macropores and water uptake by roots. The hydraulic properties of individual soil layers are parameterized according to Mualem (1976) and van Genuchten (1980). Evapotranspiration is calculated according to the approach by Shuttleworth and Wallace (1985), which differentiates between the evaporation originating from the soil or a snow cover and the transpiration and interception from a “single big leaf” plant cover, using a conductivity model. The

seasonally varying leaf area index (LAI) is an important controlling factor, which plays a key role for interception storage and the distribution of the energy available for evaporation between soil and plant, according to Lambert-Beer's law. It also has a strong influence on transpiration as it is used for upscaling canopy conductance from stomatal conductance, which varies depending on the meteorological conditions. Actual canopy conductance and available energy, in turn, determine the water demand of the vegetation cover (potential transpiration, T_p), which is covered from the soil layers depending on the layers' water availability and root length density (actual transpiration, T_a).

3.4.1.1 Climate Data, Soil and Site

LWF-Brook90 requires meteorological input data in daily resolution (precipitation, temperature, radiation, water vapour pressure, wind speed). For this model application, the data was provided by the chair of physical geography (Prof. Böhner) at the University of Hamburg using a 250×250 m grid. For methodical details see Weinzierl et al. (2013). The validation of the regionalized air temperatures shows a deviation of the monthly mean temperatures around ± 0.5 °C for 2002 and ± 0.2 °C for 2003. Monthly precipitation sums deviate on average by 5% from the measured values.

For representing the NFSI soil profiles in the model, the measured physical properties of the different depths were used and complemented with information about soil horizons, coarse soil fraction, texture and humus content from the soil profile description. Bulk density of the mineral soil was not available below 90 cm soil depth, and the measured value of the lowest layer was assigned to all subjacent horizons. Very high coarse soil fractions of bedrock horizons were constrained to 92.5% in order to include water retention in cracks and fractures in the rock. From the complete soil profile information and humus layer thickness, the model layer discretization was created, consisting of a varying number of model layers that preserve the original horizon depth boundaries and have an increasing thickness of 1–20 cm. The fine root distribution of the mineral soil model layers was derived from Eq. (3.6) (see Sect. 3.3.2), and the estimated root density of the uppermost mineral soil layer was used for the humus layer. The rooting depth was constrained to the soil depth where on-site field observations reported zero root abundance and all layers below that depth were assumed to be root-free. In case roots were observed down to the bottom of the soil profile, or not reported to the bottom of the profile, the maximum root depth was assumed to be the bottom of the soil profile, but at least 160 cm. Shallow profiles were extended correspondingly. Root penetration at profiles with limited soil depth due to solid bedrock, ground- or stagnant water was further restricted to a soil depth which was derived from soil horizon symbols following a rule-based procedure. The lower boundary of all soil profiles was formed by two standard model layers with a coarse-grained texture and an overall thickness of 40 cm in order to define a uniform lower boundary on the one hand and to facilitate upward water flow to the rooting zone even in shallow soils.

In a last step, the hydraulic properties of the mineral soil layers were derived from soil physical properties using those PTFs, which provided the most reliable predictions when compared with measured hydraulic properties (see Sect. 3.2.1). The parameters concerning the function for soil water retention according to van Genuchten (1980) (θ_s , θ_r , α , n) were derived using the PTF according to DIN 4220 (2008–2011). The parameter m was specified as $1-1/n$. The saturated conductivity (K_s) for the unsaturated conductivity model of Mualem (1976) was derived from tabular values of Wessolek et al. (2009); the parameter τ was set to 0.5. In order to derive hydraulic properties of the humus layer horizons, the PTF of Hammel and Kennel (2001) was used. Peat layers were parameterized using the PTF of Wösten et al. (1999) for organic soils. Apart from water transport in the soil matrix, for which retention and conductivity properties are relevant, the model also allowed macropore-assisted infiltration by distributing net precipitation among the humus layer and the upper 30 cm of the mineral soil with the proportions decreasing exponentially with depths.

Further variables used are latitude, slope and aspect, which determine a site's net radiation. They were taken from the header information of the NFSI II data set. The possible influence of capillary rise of water from shallow groundwater bodies to the rooting zone was not considered explicitly in the simulations.

3.4.1.2 Parameterization of the Vegetation

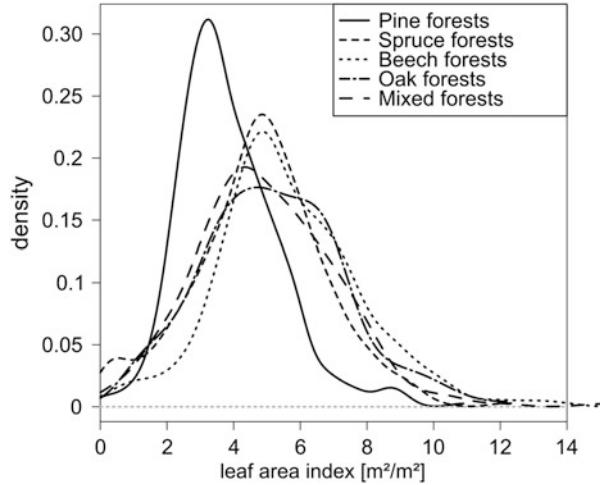
Two different approaches were chosen for the parameterization of the vegetation. In a first approach, standard parameter sets for theoretical forest stands were defined. They represent the above-ground properties [LAI, stem area index (SAI) and height] of typical stands of full-grown beech, oak, spruce, pine and mixed forests in the model (Table 3.5). The applied theoretical forest stand was determined using the

Table 3.5 Model parameters that differ depending on the forest stands in the model

	Pine	Spruce	Beech	Oak	Mixed forest
Canopy height	25	30	30	30	30
Leaf area index ($\text{m}^2 \text{m}^{-2}$) (max/min)	3.5/1.4	5.5/ 4.4	6/0.6	4.5/ 0.45	5/2
Maximum canopy conductance (mm s^{-1}) (max/min)	18/ 10.8	18/ 14.4	25/2.5	20/2	21/8.4
Canopy interception capacity (mm) (max/min)	1.63/ 0.98	1.5/ 1.2	1.2/ 0.12	1.3/ 0.13	1.1/0.44
Interception catch rate (–) (max/min)	0.41/ 0.25	0.8/ 0.64	0.92/ 0.09	0.51/ 0.05	0.8/0.32
Leaf width (cm)	0.04	0.04	0.5	5	1
Albedo (–)	0.14	0.14	0.18	0.18	0.18
Albedo, ground covered with snow (–)	0.14	0.14	0.23	0.23	0.23

Maximum and minimum values refer to intra-annual variability (summer/winter)

Fig. 3.8 Density plots of the values of leaf area index at the NFSI plots, estimated using individual tree data, shown for the different forest stand types



information about forest stand type contained in the NFSI II header information. Unspecified broadleaf forest stands were assumed to be beech stands, while unspecified coniferous forest stands were assumed to be spruce stands.

A second approach incorporates the effects of the actual forest stand (by estimating the LAI, stem area index and height) on the NFSI plots into the simulation. The results of this second application of the model are not discussed further in the context of this chapter. They are, however, made available as annual values for other evaluation groups and may be used to calculate the nutrient output with seepage water and to estimate nutrient budgets. For deriving the stem area index from the individual tree data in the harmonized forest stand inventory (HBI), the allometric functions by Hammel and Kennel (2001) were applied. The functions distinguish between broadleaf and coniferous trees. For estimating the LAI using the forest stand data, different estimation functions, depending on tree species, were used. For estimating the LAI of pines and larches, the litterfall model of Law et al. (2001) was adopted and parameterized for pine according to Ahrends et al. (2010). The leaf area of beech, oak and other broadleaf trees were estimated using the biomass functions of Weis et al. (2012). The leaf area index for spruce, fir and Douglas fir was estimated using the allometric function by Hammel and Kennel (2001), which is based on reanalyses of data on leaf mass published in Hammel and Kennel (2001). Subsequently, the estimated leaf areas of the individual trees were added together, and the forest stand LAI was calculated. The frequency distribution of the LAI estimates for various forest types is shown in Fig. 3.8 as density plot.

Apart from the forest stand properties above, both model applications (theoretical standardized forest stands and real forest stands) used the same model settings and parameters. The choice of which model parameters and model settings to use is based directly on the suggestions made by Federer et al. (2003) (albedo, light extinction coefficient), as well as the suggestions made by Hammel and Kennel (2001) (length of the foliation and leaf fall phases). Beginning and end of the growing season (i.e. bud burst in spring and start of leaf fall in autumn) were

determined dynamically for each NFSI plot using the temperature-based methods described in Menzel (1997) and von Wilpert (1991), which were parameterized for different tree species. Other parameters were adapted to fit interception evaporation measured at Level II intensive monitoring plots in Germany (ICP Forests 2010).

Because no water budget measurements exist for the NFSI plots (e.g. throughfall precipitation, soil water potential or soil water content), a direct validation of the water budget simulation cannot be carried out at the NFSI plots. However, model applications of LWF-Brook90 on intensively monitored sites and the comparison of time series collected there showed that water budget simulations using the described settings and parameters produced satisfactory results (unpublished data). In addition, the comparison between the modelled amounts of seepage water and the values taken from the Hydrological Atlas of Germany showed no systematic variations. Therefore, the assumption can be made that the model settings used provide reasonable estimates about the water budget parameters and drought stress indicators, which reflect physically and physiologically reasonable influences of climate, soil and forest stand properties.

3.4.1.3 Processing the Results

The modelled water flows [e.g. groundwater recharge (GWR), evapotranspiration (ET), actual transpiration (T_a), evaporation from interception (I) and evaporation from the soil (E)] were aggregated to time series of monthly sums and sums over the dynamic growing season for further analysis. Additionally, different drought stress indicators were derived that quantify limitations on water availability. A widely used indicator is the relative water content (RW), which is the ratio of the actual soil water storage, S_t , to the soil water storage at field capacity, FC: $RW = S_t/FC$. The relative extractable water storage, REW, is the ratio of currently plant-available water storage ($S_p = S_t - PWP$) to the plant-available water capacity, AWC: $REW = S_p/AWC$. From the depth-discrete results of the LWF-Brook90 modelling, values for S_t , S_p , RW and REW were aggregated for the following depth ranges: 0–30 cm for the mineral soil depth ($S_{t,030}$, $S_{p,030}$, RW_{030} , REW_{030}) and 0–90 cm for the effective rooting depth. Mean and minimum values over the dynamic growing season were then calculated using the daily values of the drought stress indicators in order to judge mean water availability in individual years.

Another widely used indicator for water deficiency is the difference or the ratio between actual (T_a) and potential transpiration (T_p). A decrease in T_a below T_p is caused by limited water availability in the root space in LWF-Brook90. The transpiration ratio, $Tratio = T_a/T_p$, with values of <1 , and the transpiration difference, $Tdiff = T_p - T_a$, with values of >0 , therefore indicate a water shortage in the root space.

From the annual and growing season total water flows and drought stress indicators, distribution statistics (mean, median, quartile, minimum, maximum) for the period 1981–2010 were calculated for each NFSI plot. Also, the relative deviation of the annual values from the mean value in the period 1961–1990 was calculated for each NFSI plot in order to examine time-related changes with the

help of distribution statistics (median, quartile, 90%- and 10%-quantile for each year over all NFSI plots).

3.4.2 Results

Figure 3.9 shows distribution statistics of evapotranspiration during the growing season (ET, Fig. 3.9a), annual total groundwater recharge (Fig. 3.9b), transpiration difference (TDIFF, Fig. 3.9c) and mean relative extractable soil water storage in the rooting zone during growing season (REW, Fig. 3.9d) at the NFSI plots, modelled using the standardized forest stand. It shows the cumulative frequency distribution of the medians, as well as the respective ranges and quartiles of the individual annual values of NFSI plots for the period 1981–2010. The spatial distribution of the medians of these dimensions is shown as a map in Fig. 3.10.

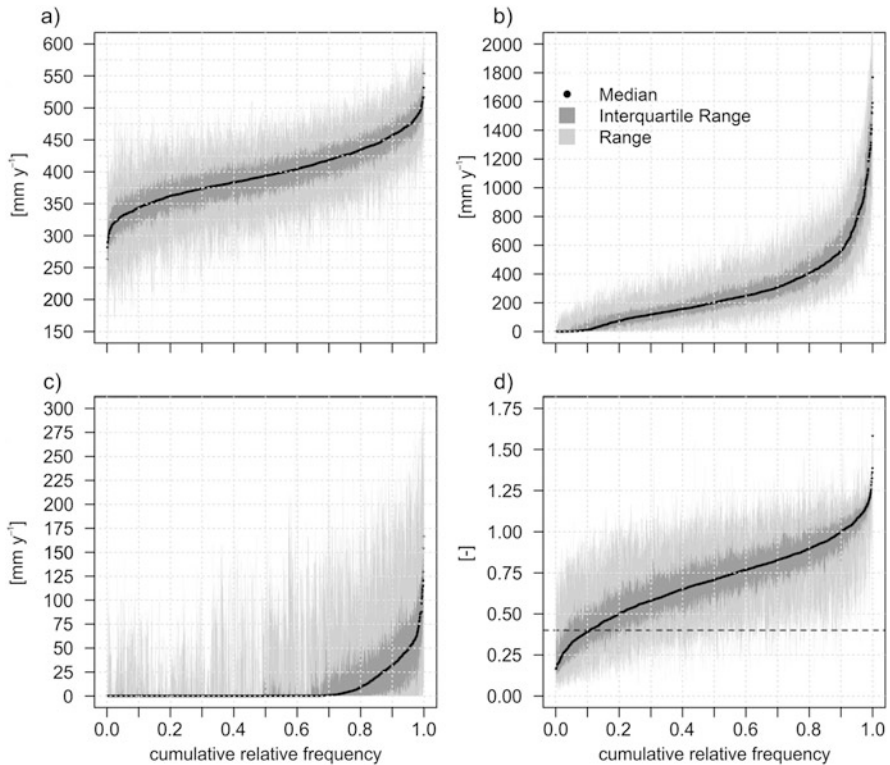


Fig. 3.9 Median values of the actual evapotranspiration during growing season (a), the annual groundwater recharge (b), the transpiration difference during growing season (c) and the mean relative available soil water storage during growing season (d) for NFSI plots in the period 1981–2010; modelled with standardized forest stands

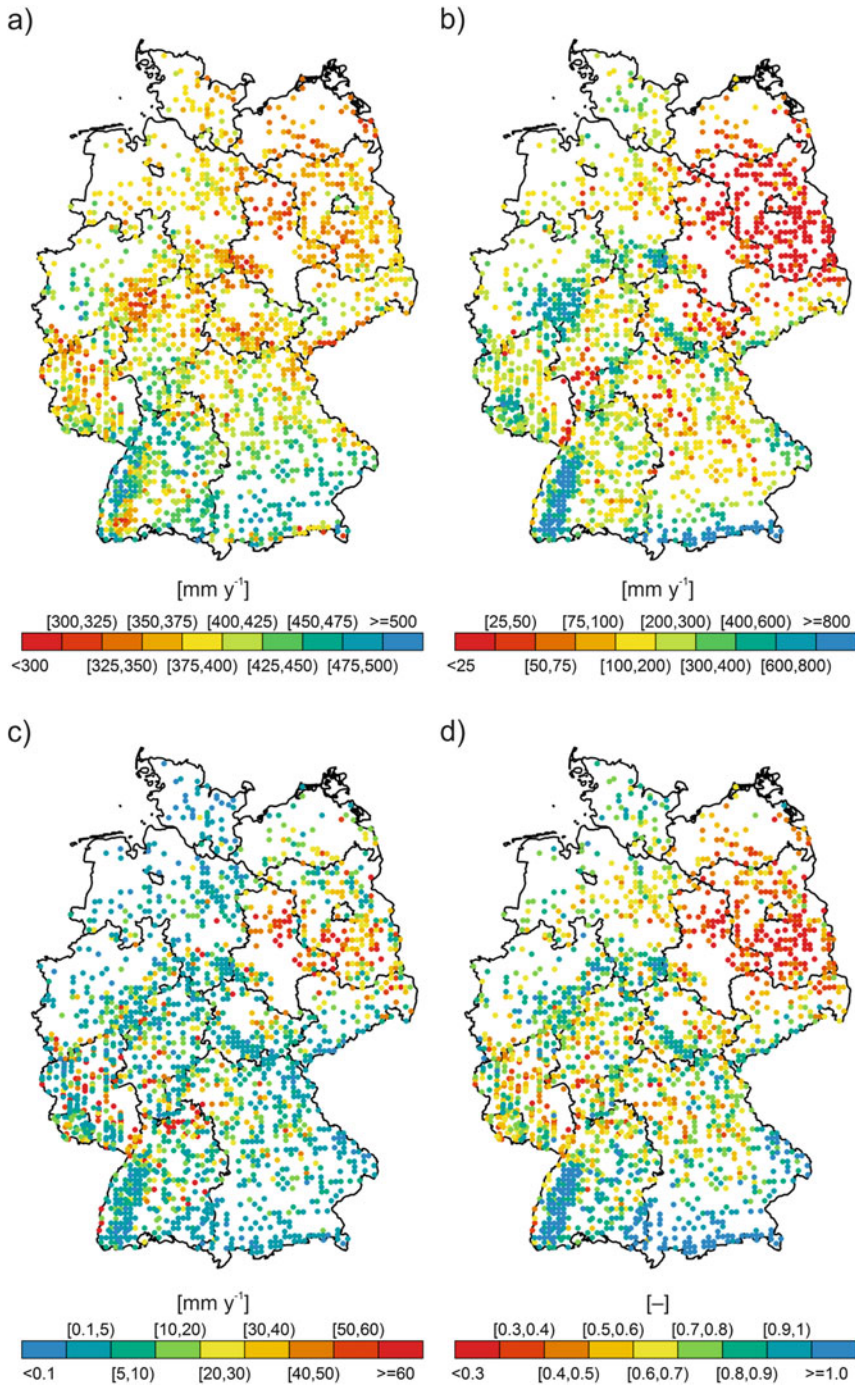


Fig. 3.10 Spatial distribution of the median values of the actual evapotranspiration during growing season (a), the annual groundwater recharge (b), the transpiration difference during growing season (c) and the mean relative available soil water storage during growing season (d) for NFSI plots in the period 1981–2010; modelled with standardized forest stands

Figure 3.9a shows that the mean actual evapotranspiration during the growing season of 80% of the NFSI plots lies between 350 and 450 mm. Plots especially with lower mean evaporation have extreme fluctuations, with up to 300 mm between individual years of the represented period (1981–2010). But in half of all years, the fluctuation lies below 60 mm which is the mean difference between the upper and the lower quartile over all plots. About 5% of the NFSI plots show mean evapotranspiration rates of 475 mm or more (Fig. 3.9a). These can be found in the Bavarian late-moraines and molasses and in the foothills of the Alps and the Black Forest (Fig. 3.10a; blue and blue-green dots). High evaporation rates of 450 mm or more can also be found on the western slopes of the Pfälzerwald and Odenwald and in the Bergische Land. On the one hand, the mentioned regions have very high precipitation. On the other hand, they are also warm with high potential evaporation rates that take effect during long growing seasons. The lowest evapotranspiration rates do not show such a distinct geographical pattern. Several areas in the rain shadows of mountain ranges (north-eastern foothills of the Harz, Altmark, Hessisches Schiefergebirge) are distinguishable, and it seems that there is an increase of NFSI plots with less than 350 mm evapotranspiration (yellow, orange and red dots) towards the north. But plots with very low evapotranspiration of less than 300 mm appear more or less scattered everywhere on the map, thereby blurring spatial patterns. On these plots, actual transpiration is substantially limited each year due to a high skeletal fraction and/or shallow tree rooting. Apart from those sites, the mean evapotranspiration follows the interaction between precipitation and temperature. In this way, a site in the cool and moist Hochsauerland (precipitation/temperature during growing season, 420 mm/13 °C) with an average evapotranspiration that is limited by rather low potential transpiration can have the same low evaporation of less than 350 mm as a warm and dry site (250 mm/16.5 °C) in Brandenburg or Saxony-Anhalt during the summer half of the year. There, the low evapotranspiration rate is caused by low precipitation and the low water retention capacity of the typically sandy soils. The transpiration difference (Tdiff, Fig. 3.10c) makes it possible to determine whether or not a site's evaporation is limited by water shortage. Tdiff in the growing season is higher than 30 mm on average in southern Brandenburg and smaller than 5 mm in the Hochsauerland and other top ranges of low mountain ranges and in the proximity of the North Sea. Overall, growing season Tdiff on all NFSI sites is characterized by a large range (Fig. 3.9c), illustrating that water shortage may occur in all plots during dry years in which the vegetation's water demand cannot be entirely met through water reserves in the soil.

About 25% of the NFSI plots show a mean annual groundwater recharge of less than 100 mm (Fig. 3.9b), 10% of the plots have very little groundwater recharge. There, the median is at 0 mm, which means that in half of the years from 1981 to 2010, the groundwater has not been recharged at all for the assumed theoretical forest stand. For most plots, annual groundwater recharge is 50–400 mm, but a substantial decrease in, or even a complete absence of, groundwater recharge in extreme years is possible. Approx. 10% of the plots have a discharge of more than 500 mm per year; it can be as high as 2400 mm in some years, e.g. at sites at high altitude and with high precipitation, where snow masses accumulate in winter and

melt in spring. While the actual evapotranspiration during growing season is mainly a product of temperature and precipitation, groundwater recharge clearly follows the precipitation distribution (Fig. 3.10b). Plots with an annual groundwater recharge of more than 400 mm are located—almost without exception—in high altitudes with high precipitation. Large areas with very low (<25 mm) groundwater recharge are located mainly in Brandenburg and Saxony-Anhalt, and smaller areas are situated in eastern Thuringia, southern Hesse and the Rhine-Main area (Fig. 3.10b), all of which experience very low annual rainfall amounts and high potential evaporation.

Figure 3.9d shows the cumulative frequency distribution of the mean available soil water storage in the root space during growing season. It becomes clear that the NFSI plots have a wide range. Approx. 10% of the sites have a mean available soil water storage of more than 100% of the AWC. On the one hand, soil horizons with low hydraulic conductivity cause infiltrating water to accumulate in the root space, so that the FC is regularly exceeded on these sites. On the other hand, large amounts of precipitation provide a positive water balance also during growing season and therefore make sure that loss through transpiration is regularly compensated by abundant precipitation. On approx. 10% of the NFSI plots, however, the mean available soil water storage decreased to below 40% of the maximum value (AWC) in at least half, on 5% of the NFSI plots in three-fourths of the years in the period 1981–2010. Falling below this threshold (drawn in as a reference line in Fig. 3.9d) is interpreted as a water shortage by Bréda and Granier (1996). It occurs mainly on NFSI plots that get low amounts of precipitation during growing season on the one hand, or whose available water capacity is limited by a high skeletal fraction or a shallow rooting on the other hand. Such NFSI plots are mainly found in parts of Brandenburg, Thuringia and Saxony-Anhalt but also scattered in the low mountain ranges on particularly shallow sites. On most NFSI plots, water shortage only occurs in dry years. However, for approx. 90% of the NFSI plots during the period 1981–2010, mean available water retention falls below the Granier threshold of 40% AWC for at least one growing season.

3.5 Deriving the Risk for Drought Stress

The probability of falling below the limit values of soil water availability relevant to tree physiology, such as the threshold value according to Bréda and Granier (1996), is a key indicator for predicting tree damage caused by climate change. In the following, the results of the simulation with LWF-Brook90 are aggregated to get characteristic values for water shortage. They are linked to tree growth observed at the NFSI plots in Chap. 11.

3.5.1 Characteristic Properties of Water Shortage

In addition to the characteristic properties of water shortage defined in Sect. 3.4.1.3, other indicators are derived below, which quantify the intensity and duration of periods with water shortage. The characteristic value d_REW_{CL} indicates the number of days, on which the relative soil water storage (REW) falls below a certain critical limit (CL_{REW}) during growing season; v_REW_{CL} indicates the missing water volume below the threshold value:

$$v_REW_{CL} = \sum_{i=\text{vegbe}}^{\text{vegend}} \begin{cases} S_{p,i}/aFC < CL_{REW} : 1 - (S_{p,i}/aFC)/CL_{REW} \\ S_{p,i}/aFC \geq CL_{REW} : 0 \end{cases} \quad (3.9)$$

$$d_REW_{CL} = \sum_{i=\text{vegbe}}^{\text{vegend}} \begin{cases} S_{p,i}/aFC < CL_{REW} : 1 \\ S_{p,i}/aFC \geq CL_{REW} : 0 \end{cases} \quad (3.10)$$

For further evaluation, three different threshold values were tested: $CL_{REW} = 0.2$, 0.4 and 0.6.

Similarly, drought stress indicators based on threshold values were also calculated using transpiration ratios according to the following equations:

$$v_Tratio_{CL} = \sum_{i=\text{vegbe}}^{\text{vegend}} \begin{cases} T_a/T_p < CL_{Tratio} : 1 - (T_a/T_p)/CL_{Tratio} \\ T_a/T_p \geq CL_{Tratio} : 0 \end{cases} \quad (3.11)$$

$$d_Tratio_{CL} = \sum_{i=\text{vegbe}}^{\text{vegend}} \begin{cases} T_a/T_p < CL_{Tratio} : 1 \\ T_a/T_p \geq CL_{Tratio} : 0 \end{cases} \quad (3.12)$$

The critical limits used were $CL_{Tratio} = 0.8$ and $CL_{Tratio} = 0.5$.

Further drought stress indicators were derived from the soil water potential in the root space. For this purpose, the mean soil water potential (ψ_w) (weighted by layer thickness) for the root space was calculated, and the days during growing season were counted on which ψ_w fell below the threshold value $CL_{\psi} = -1200$ hPa (von Wilpert 1991). Also, a “deficit” (integral of the time series of water potential below CL_{ψ}) was defined similar to v_REW_{CL} :

$$v_def_{CL} = \sum_{i=\text{vegbe}}^{\text{vegend}} \begin{cases} \psi_w < CL_{\psi} : CL_{\psi} - \psi_w \\ \psi_w \geq CL_{\psi} : 0 \end{cases} \quad (3.13)$$

$$d_def_{CL} = \sum_{i=\text{vegbe}}^{\text{vegend}} \begin{cases} \psi_w < CL_{\psi} : 1 \\ \psi_w \geq CL_{\psi} : 0 \end{cases} \quad (3.14)$$

The amount of deep seepage water below the root space ($vrfln$) was considered as a measure for possible water surplus. In addition to the output parameters of LWF-Brook90, different climatic parameters were examined in regard to their influence on growth in thickness of the trees: air temperature (mean value $tmean$, temperature sum $tsum$, minimum $tmin$), number of days that exceed a temperature threshold of 5, 10

or 20 °C ($gdd5$, $gdd10$, $gdd20$), as well as respective temperature sums ($tsum5$, $tsum10$, $tsum20$), precipitation ($prec$), global radiation ($globrad$), FAO grass reference evapotranspiration ($et0$), climatic water budget (kwb), beginning, end and length of the growing season (vp_start , vp_end , vp_dauer). Annual values for all parameters were derived from the modelling. They are either calculated as the mean values/sums of the whole year (ending of the variable is $_y$), of the dynamic growing season of this year which was calculated using LWF-Brook90 ($_vp$), of the months April–September or of the months May–July.

3.5.2 Future Drought Trend

It was shown that soil water availability has substantial influence on the width of year rings of the different trees examined. With the exception of the BRT model for oak, the extent of dry periods with a soil water potential of less than -1200 hPa in the root space $v_Psi_{w1200_vp}$ (see Eq. 3.13) was an important covariate in the BRT models of all tree species. In the following, the results of the LWF-Brook90 modelling are presented in regard to the space-time dynamic of the water shortage index $d_Psi_{w1200_vp}$ which correlates strongly with $v_Psi_{w1200_vp}$, but which is, in contrast, specified by a descriptive unit (number of days during growing season where the value falls below the limit). Figure 3.11 shows the annual values for $d_Psi_{w1200_vp}$ at each NFSI plot for the period 1961–2013, where the red symbols represent intensive water shortage and the blue symbols represent plots where the critical value of -1200 hPa was not exceeded throughout the vegetation period. In extremely dry years (1976, 2003), the modelling shows that nearly all NFSI plots fall—in part substantially and for a very long time—below the critical soil water potential. A distinct spatial pattern of the modelled water shortage can be noticed in medium years. There are two types of areas which have particularly intensive water shortage: the stony soils in the low mountain ranges, where the transpiration of the plants uses up the AWC quickly due to high rock content, and the regions located in rain shadows of mountains (e.g. east of the Harz, Thüringer Becken). Looking at the model results for the individual years, the year 1989 seems to mark a turning point in the water supply of forest stands. Since the beginning of the 1990s, years with increased water stress have been on the rise. Of the 10 years with the best water supply—meaning the highest percentage of plots without water stress ($d_Psi_{w1200_vp} = 0$)—there is only one after 1990. For four of the years within the decade from 1970 to 1979, the median of $d_Psi_{w1200_vp}$ across all plots lies below the long-time median, which means that 4 of the 10 years are dryer than average. This value is particularly low for the decade 1980–1989 (3 out of 10 years) and is increasing ever since (1990–1999, 7 out of 10 years; 2000–2009, 6 out of 10 years; 2010–2013, 3 of the 4 years). In addition to the increasing number of particularly dry years, the results of the model show a tendency towards a decrease in variance between the NFSI plots. This can be attributed to plots that usually have a

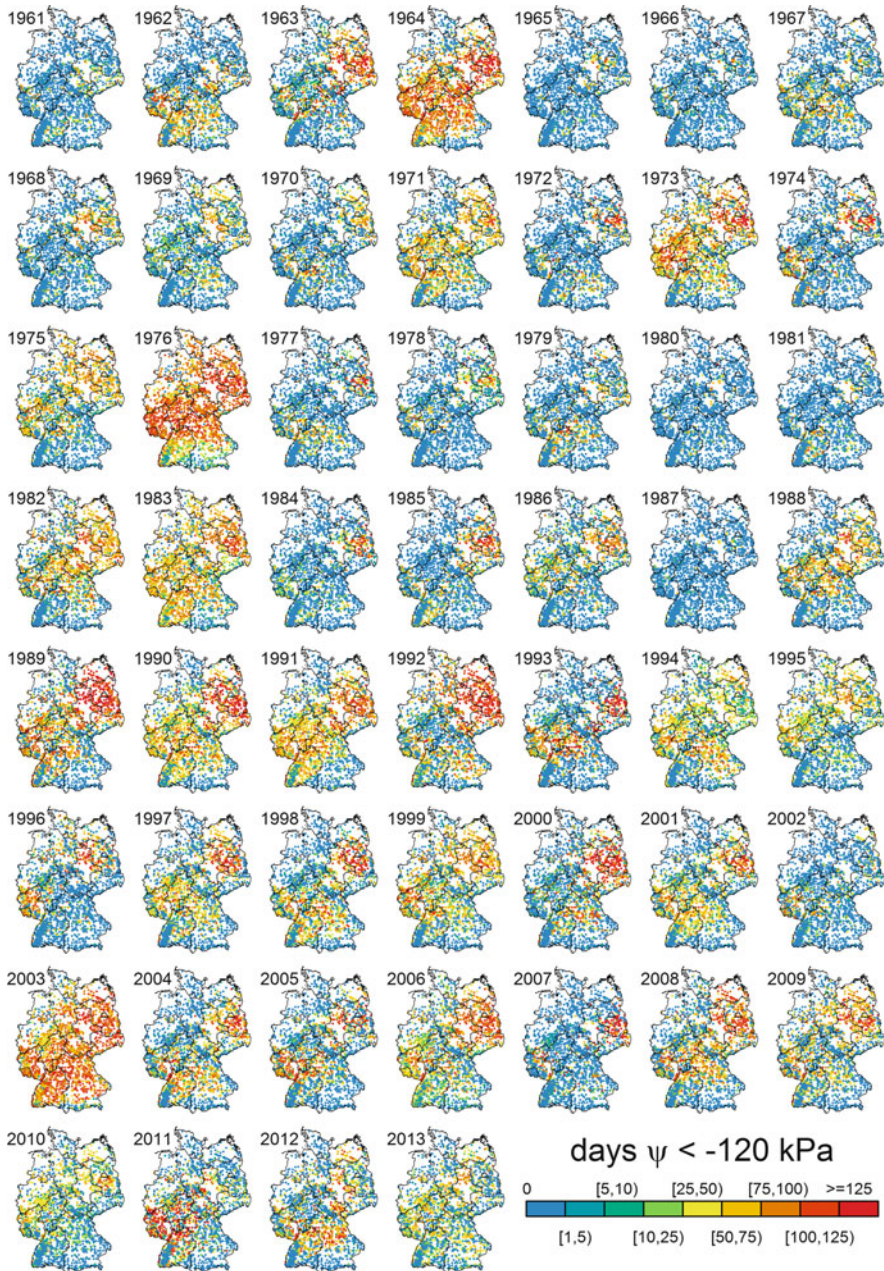


Fig. 3.11 Water shortage index $d_{\Psi}w_{1200_{\psi p}}$ (Eq. 3.14), derived from LWF-Brook90 modelling for the years 1961–2013, which quantifies the shortfall below a critical matric potential ($CL_{\psi} = -1200$ hPa) in the root space

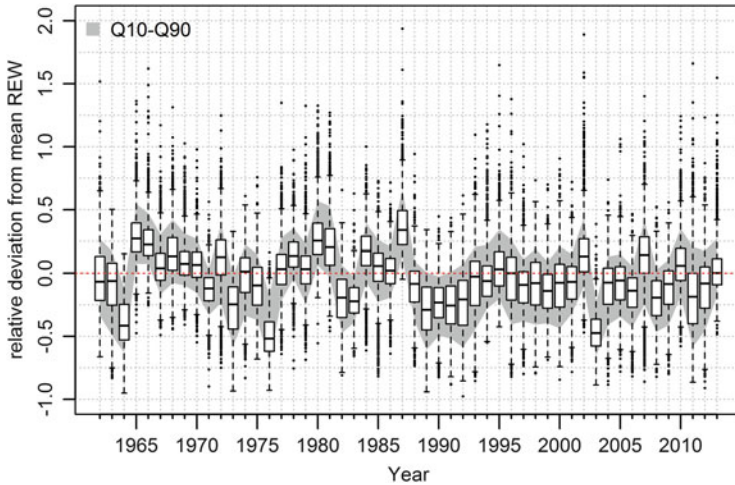


Fig. 3.12 Distribution statistics (medians, quartile areas, 10%- and 90%-quantile) of the available soil water storage during growing season, shown as relative deviation from the long-term mean value of the period 1961–1990

good water supply but experience drought stress in the second half of the simulation period.

The long-term trend of periods of water shortage in the root space also becomes clear in Fig. 3.12, where the chronological trend of the available water storage (REW_{WReff_vp}) is shown as a distribution statistics of the relative deviation from the reference period 1961 to 1990. Years that were exceptionally moist or dry during growing season compared to the reference period can be identified in this way. The general trend of an increasing number of growing seasons with below-average water supply since the end of the 1980s can also be seen here. In most years since 1989, the median was negative, which shows that a below-average soil water storage was registered here for most NFSI plots, compared to 1961–1990. In the time from 1989 to 1992, even the 90%-quantile is negative. This means that 90% of the NFSI plots in four consecutive growing seasons showed a below-average water supply. A fourth of the plots had a soil water storage which was 25% lower compared to the reference period. In the extremely dry years 1976 and 2003, as many as 75% of the NFSI plots had a water storage which was at least 25% less than average. Since 1988, only in the 5 years 1995, 2002, 2007, 2010 and 2013 were the medians of the available water storage clearly above the reference value of the period 1961–1990, while in 20 years, they were clearly below that value.

3.6 Summary and Conclusions

By reprocessing and combining soil, root and forest stand parameters, it was possible to make reliable estimates about the governing factors for the water budget on the individual NFSI plots and to parameterize the one-dimensional water budget model LWF-Brook90 based on this. Special attention was paid to the evaluation of PTFs used for estimating soil hydraulic properties and to the identification of those functions that best represent the complete value range of the very heterogeneous NFSI data set. The decision was made in favour of the PTF according to DIN 4220 (2008–2011) for estimating the van Genuchten parameters, and the PTF by Wessolek et al. (2009) for estimating the FC, AWC and PWP, although the PTF by Puhlmann and von Wilpert (2011) produced the best and most stable estimates for all textures except the sands.

A similarly intensive evaluation was carried out for estimating the relative depth distribution of roots based on data from root estimates and root counting at the NFSI profiles. A multivariate BRT model was created that is able to explain the depth distribution of fine roots (<2 mm) by the determining factors soil depth, humus content, bulk density, slope and AWC. What was unexpected was that there were largely no dependencies on forest stand type and the degree of acidification (depth profile of base saturation) and only a weak dependency on the soil type. Those are the determining factors that are formally attributed to have a significant influence on the rooting depth. A possible explanation for the rooting intensity not being consistent with the hypothesis could be that the chemical site properties are levelled out by acidification of the soil to such an extent that both tree species and trophy of the sites do not have a differentiating effect on the depth profiles of fine roots anymore, and therefore only distinct differences in soil physics and soil structure (TRD, slope inclination, AWC, humus content) are distinguishable.

On the basis of these input parameters, two versions of water budget modelling were carried out using LWF-Brook90. They are different in the treatment of vegetation properties—one version was calculated using regionally adapted standardized forest stand properties (beech, oak, spruce, pine and mixed stands) to focus on the soil properties that diversify the water budget. In a second version, the LAI, the roughness of the bark and the height were taken from the forest stand information at a NFSI point in order to represent the actual drought stress occurring at that point as realistically as possible. All modelling was carried out in daily resolution, so that target variables such as seepage water output, change in soil water storage, evapotranspiration, etc. are available in daily resolution or coarser and so that those variables may be used for applications such as seepage water predictions for contaminant and nutrient output, water availability for the parameterization of climate-sensitive growth models or analysis of the significance of dry years for tree growth and forest health. The emphasis of the examination in this chapter was on the derivation and evaluation of characteristic drought stress variables. The time series of available soil water storage and different drought stress indices conformably show that the intensity of water shortage increased since 1990 and that from

then on, years with good water supply occurred only sporadically, while before, years in which the soil water storage was above- or below-average existed in equal parts.

To empirically evaluate the impact of drought on tree growth, the deciding factor is not only the water deficit but also timing, duration and intensity of the drought. For identical weather conditions, not only the tree species but especially also the soil with its retention capacity determine the extent to which droughts can develop. Experiments on young beech and oak trees prove that trees experience acute drought stress when the soil water availability falls below 20%, which can eventually lead to their death.

References

- Ad-Hoc AG–Boden (ed) (2005) *Bodenkundliche Kartieranleitung (KA 5)*, vol 5. Schweizerbart'sche Verlagsbuchhandlung, Stuttgart
- Ahrends B, Meesenburg H, Döring C, Jansen M (2010) A spatio-temporal modelling approach for assessment of management effects in forest catchments. Status and perspectives of hydrology in small basins. IAHS, Goslar-Hahnenklee
- AK Standortskartierung (2003) *Forstliche Standortsaufnahme: Begriffe, Definitionen, Einteilungen, Kennzeichnungen, Erläuterungen*, 6th edn. IHW-Verlag, Eiching near Munich
- Bréda N, Granier A (1996) Intra- and interannual variations of transpiration, leaf area index and radial growth of a sessile oak stand (*Quercus petraea*). *Annales Des Sciences Forestieres* 53 (2–3):521–536. <https://doi.org/10.1051/forest:19960232>
- de Camargo AP, Sentelhas PC (1997) Performance evaluation of different methods for estimating potential evapotranspiration in the state of Sao Paulo, Brazil – an analytical review of potential evapotranspiration. *Revista Brasileira de Agrometeorologia* 5(1):89–97
- DIN 4220 (2008–2011) *Bodenkundliche Standortbeurteilung – Kennzeichnung, Klassifizierung und Ableitung von Bodenkennwerten (normative und nominale Skalierung)*
- Elith J, Leathwick JR, Hastie T (2008) A working guide to boosted regression trees. *J Anim Ecol* 77 (4):802–813. <https://doi.org/10.1111/j.1365-2656.2008.01390.x>
- Federer CA, Vörösmarty C, Fekete B (2003) Sensitivity of annual evaporation to soil and root properties in two models of contrasting complexity. *J Hydrometeorol* 4(6):1276–1290. [https://doi.org/10.1175/1525-7541\(2003\)004<1276:soaets>2.0.co;2](https://doi.org/10.1175/1525-7541(2003)004<1276:soaets>2.0.co;2)
- Gale M, Grigal D (1987) Vertical root distributions of northern tree species in relation to successional status. *Can J For Res* 17(8):829–834
- Gauer J, Kroiher F (2012) *Waldökologische Naturräume Deutschlands – Forstliche Wuchsgebiete und Wuchsbezirke – Digitale Topographische Grundlagen – Neubearbeitung Stand 2011*. Landbauforschung vTI Agriculture and Forestry Research, Braunschweig
- Hammel K, Kennel M (2001) *Charakterisierung und Analyse der Wasserverfügbarkeit und des Wasserhaushalts von Waldstandorten in Bayern mit dem Simulationsmodell BROOK90*. Forstliche Forschungsberichte München, vol 185. Technische Uni München Wissenschaftszentrum Weihenstephan, Munich
- Hangen E, Scherzer J (2004) *Ermittlung von Pedotransferfunktionen zur rechnerischen Ableitung von Kennwerten des Bodenwasserhaushalts (FK, PWP, nFK, kapillarer Aufstieg)*. Bundesministerium für Verbraucherschutz, Ernährung und Landwirtschaft (BMVEL), Bonn
- Hartmann P, von Wilpert K (2014) Fine-root distributions of central European forest soils and their interaction with site and soil properties. *Can J For Res* 44(1):71–81. <https://doi.org/10.1139/cjfr-2013-0357>

- Hartmann P, von Wilpert K (2016) Statistisch definierte Vertikalgradienten der Basensättigung sind geeignete Indikatoren für den Status und die Veränderungen der Bodenversauerung in Waldböden. *Allgemeine Forst- und Jagdzeitung* 187(3/4):61–69
- ICP Forests (2010) Manual on methods and criteria for harmonized sampling, assessment, monitoring and analysis of the effects of air pollution on forests. UNECE, ICP Forests, Hamburg
- Law BE, Van Tuyl S, Cescatti A, Baldocchi DD (2001) Estimation of leaf area index in open-canopy ponderosa pine forests at different successional stages and management regimes in Oregon. *Agric For Meteorol* 108(1):1–14. [https://doi.org/10.1016/s0168-1923\(01\)00226-x](https://doi.org/10.1016/s0168-1923(01)00226-x)
- Mellert KH, Rückert G, Weis W, Tiemann J, Brendel J (2009) Validierung von Pedotransferfunktionen – Zebris Projektbericht 2.0. Johann Heinrich von Thünen Institut (TI)
- Menzel A (1997) Phänologie von Waldbäumen unter sich ändernden Klimabedingungen – Auswertung der Beobachtungen in den Internationalen Phänologischen Gärten und Möglichkeiten der Modellierung von Phänodaten. Technische Universität München, Wissenschaftszentrum Weihenstephan, Munich
- Mualem Y (1976) A new model for predicting the hydraulic conductivity of unsaturated porous media. *Water Resour Res* 12(3):513–522
- Puhlmann H, von Wilpert K (2011) Test und Entwicklung von Pedotransferfunktionen für Wasserretention und hydraulische Leitfähigkeit von Waldböden. *Waldökologie, Landschaftsforschung und Naturschutz* 12:61–71
- Puhlmann H, von Wilpert K (2012) Pedotransfer functions for water retention and unsaturated hydraulic conductivity of forest soils. *J Plant Nutr Soil Sci* 175(2):221–235. <https://doi.org/10.1002/jpln.201100139>
- Puhlmann H, von Wilpert K, Lukes M, Dröge W (2009) Multistep outflow experiments to derive a soil hydraulic database for forest soils. *Eur J Soil Sci* 60(5):792–806. <https://doi.org/10.1111/j.1365-2389.2009.01169.x>
- Russ A, Riek W (2011) Pedotransferfunktionen zur Ableitung der nutzbaren Feldkapazität – Validierung für Waldböden des nordostdeutschen Tieflands. *Waldökologie, Landschaftsforschung und Naturschutz* 11:5–17
- Schramm D, Schultze B, Scherzer J (2006) Validierung von Pedotransferfunktionen zur Berechnung von bodenhydrologischen Parametern als Grundlage für die Ermittlung von Kennwerten des Wasserhaushaltes im Rahmen der BZE II. Technical Report, TU Bergakademie Freiberg und UDATA-Umweltschutz und Datenanalyse im Auftrag des Bundesministerium für Ernährung, Landwirtschaft und Verbraucherschutz (BMELV)
- Shuttleworth WJ, Wallace JS (1985) Evaporation from sparse crops – an energy combination theory. *Q J R Meteorol Soc* 111(469):839–855. <https://doi.org/10.1256/smsqj.46909>, <https://doi.org/10.1002/qj.49711146910>
- Teepe R, Dilling H, Beese F (2003) Estimating water retention curves of forest soils from soil texture and bulk density. *J Plant Nutr Soil Sci* 166(1):111–119. <https://doi.org/10.1002/jpln.200390001>
- van Genuchten MT (1980) A closed-form equation for predicting the hydraulic conductivity of unsaturated soils. *Soil Sci Soc Am J* 44(5):892–898
- Vereecken H, Maes J, Feyen J, Darius P (1989) Estimating the soil moisture retention characteristic from texture, bulk density, and carbon content. *Soil Sci* 148(6):389–403
- von Wilpert K (1991) Intraannual variation of radial tracheid diameters as monitor of site specific water stress. *Dendrochronologia* 9:95–113
- von Wilpert K, Hildebrand EE (1997) Kaliummangel in Wäldern durch selektive Kaliumverarmung von Aggregatoberflächen. *Mitteilungen der Deutschen Bodenkundlichen Gesellschaft* 85(1):449–452
- Weinzierl T, Conrad O, Böhner J, Wehberg J (2013) Regionalization of baseline climatologies and time series for the Okavango catchment. *Biodiversity & Ecology* 5:235–245
- Weis W, Hertel C, Wagner A, Raspe S (2012) Abschlussbericht ST 241 – Verbesserung der Wasserhaushaltsmodellierung mit Daten des forstlichen Umweltmonitorings im Projekt FUTMON (LIFE+). Landesanstalt für Wald und Forstwirtschaft (LWF), Freising

- Wessolek G, Kaupenjohann M, Renger M (2009) Bodenphysikalische Kennwerte und Berechnungsverfahren für die Praxis. Rote Reihe, vol 40. TU Berlin, Institut für Ökologie, Fachgebiet Bodenkunde, Standortkunde und Bodenschutz, Berlin
- Wösten JHM, Lilly A, Nemes A, Le Bas C (1999) Development and use of a database of hydraulic properties of European soils. *Geoderma* 90(3–4):169–185. [https://doi.org/10.1016/s0016-7061\(98\)00132-3](https://doi.org/10.1016/s0016-7061(98)00132-3)
- Zirlewagen D, von Wilpert K (2011) Regionalisierung bodenphysikalischer Eingangsgrößen für bodenhydraulische Pedotransferfunktionen. *Waldökologie, Landschaftsforschung und Naturschutz* 12:73–83

Open Access This chapter is licensed under the terms of the Creative Commons Attribution 4.0 International License (<http://creativecommons.org/licenses/by/4.0/>), which permits use, sharing, adaptation, distribution and reproduction in any medium or format, as long as you give appropriate credit to the original author(s) and the source, provide a link to the Creative Commons licence and indicate if changes were made.

The images or other third party material in this chapter are included in the chapter's Creative Commons licence, unless indicated otherwise in a credit line to the material. If material is not included in the chapter's Creative Commons licence and your intended use is not permitted by statutory regulation or exceeds the permitted use, you will need to obtain permission directly from the copyright holder.

